# PREDICTION AND COMPARISON OF *IN SITU* ACOUSTIC PRESSURE LEVELS FOR LINEARLY DERATED FIELDS AND NONLINEAR TISSUE FIELDS

BY

DARSHAN RAMAN GANDHI

B.S., University of Illinois, 1991

THESIS

Submitted in partial fulfillment of the requirements
for the degree of Master of Science in Electrical Engineering
in the Graduate College of the
University of Illinois at Urbana-Champaign, 1993

Urbana, Illinois

# ABSTRACT

Nonlinear wave propagation plays an important role in medical ultrasound due to the high acoustic pressure amplitude levels employed. Measurements to comply with labeling standards and FDA requirements for diagnostic equipment are performed in water, a medium readily available and easy to use. To predict the fields in tissue, an attenuating and absorbing medium, the FDA has established a derating factor of 0.3 dB/cm-MHz. This model, however, is based on a simple linear model which does not take into account the nonlinearity of the medium nor does it consider the effects of diffraction. This thesis provides some implications when these effects are taken into account. The Khokhlov-Zabolotskaya-Kuznetsov (KZK) model for nonlinear thermoviscous diffractive waves is developed. Using this model, the acoustic pressure amplitudes along the beam axis for the fundamental and the second and third harmonics are examined for a plane piston transducer of uniform excitation with an initially sinusoidal source frequency of 2.25 MHz. First, a nonlinear field using the KZK model is generated in water, and subsequently the linear derating factor is applied to estimate the *in situ* fields in tissue. This result is then compared to the nonlinear fields generated with the KZK model but now using tissue parameters to compare the two schemes used to estimate *in situ* exposure. Due to the presence of nonlinearities, the dissipation of energy due to attenuation, and acoustic saturation, the FDA derating underestimates the output pressure fields in tissue using simulations based on the KZK model.

# DEDICATION

This thesis is dedicated to my parents, Raman and Padma Gandhi, and to my brother, Bhai, who have given all their support in all my endeavors. Whenever there is doubt, they are always there to motivate and encourage me to continue on ...

# ACKNOWLEDGEMENTS

My thanks go to my advisor, Professor William D. O'Brien, Jr., for his enthusiasm, encouragement, guidance, and patience and for the opportunity to achieve this goal. I would like to thank the wonderful people at the Bioacoustic Research Laboratory, especially Billy McNeill, Bob Cicone, Kay Carnes, and Wanda Elliot, for all of their help and pleasant conversations. I would like to express sincere gratitude to my friends: Tzuping and Dan for the walks, Eric and Scott for their advice, Dave and Sonoko for their encouragement, and especially to Beth Haken, for listening. Finally, I would like to give a special thanks to my friends in absentia: Linda, Ilmar, Jae, Greg, Aamir, and Kaz who have helped me to maintain my insanity.

# TABLE OF CONTENTS


| CHAPTER | | PAGE |
|---|---|---|
| 1 | INTRODUCTION | 1 |
| 2 | ULTRASONIC EXPOSURE | 4 |
| | 2.1 Principles of Ultrasound | 4 |
| | 2.2 Biological Effects | 7 |
| | 2.3 Output Labeling | 9 |
| | 2.4 Tissue Derating | 11 |
| 3 | NONLINEAR WAVE PROPAGATION | 13 |
| | 3.1 Nonlinear Processes | 13 |
| | 3.2 Dissipation | 17 |
| | 3.3 Stages of Propagation | 19 |
| | 3.4 Models | 22 |
| 4 | THE KZK EQUATION | 23 |
| | 4.1 KZK Model | 23 |
| | 4.2 Numerical Solution | 24 |
| | 4.3 Boundary Conditions | 26 |
| | 4.4 Numerical Implementation | 27 |
| 5 | SIMULATIONS | 30 |
| | 5.1 Tissue Derating | 30 |
| | 5.1.1 Linear case, $p_s$ = 25 kPa | 33 |
| | 5.1.2 Moderate amplitude case, $p_s$ = 250 kPa | 40 |
| | 5.1.3 High amplitude case, $p_s$ = 2.50 MPa | 45 |
| | 5.2 Discussion | 50 |
| 6. | CONCLUSIONS | 51 |
| | REFERENCES | 53 |
| | APPENDIX A KZK SIMULATION PROGRAMS | 56 |

# CHAPTER 1
# INTRODUCTION

The primary aim of this thesis is to study current calibration procedures when finite amplitude wave propagation is considered. Acoustic pressure fields generated in a water medium that are derated based on linear methods may not adequately describe the acoustic pressure fields in tissue especially at higher acoustic pressure levels.

Accurate acoustic field propagation models are necessary to determine the *in situ* exposure levels for the purpose of assessing safety requirements of diagnostic equipment. Ultrasonic energy is absorbed by tissue where high intensities have the possibility of inducing biological effects due to heating and cavitation although no damage has been reported from clinical examinations [1].

Current calibration procedures are conducted in a water medium in which a hydrophone is used to measure the acoustic pressure from which the intensity fields are calculated. An estimate of the *in situ* intensity levels is subsequently performed by applying a derating factor as established by the Food and Drug Administration [20]. A problem with the derating scheme is that the FDA does not take into account nonlinear propagation which may result in an incorrect estimate of the acoustic pressures and intensities.

The propagation of acoustic waves can be considered linear as long as the amplitude is sufficiently small. However, Carstensen et al. demonstrated the presence of nonlinear fields for the intensities and frequencies employed in diagnostic ultrasound [5]. That is, as a finite amplitude wave is emitted in a water medium, the temporal acoustic pressure waveform will begin to distort and generate harmonic frequency components. The extent of nonlinear effects is related not only to the source acoustic pressure but is also dependent on the characteristics of the media. Water is a nonlinear medium which possesses low attenuation so that significant waveform distortion will occur at high acoustic pressure values. Biological tissue also exhibits nonlinearities as discussed by Haran and Cook except that a tissue medium possesses higher

attenuation which is almost linear with frequency while water is low loss with a quadratic dependence of attenuation on frequency [9]. As a result, measurements conducted in water do not reflect *in situ* exposure. Instead, experimental techniques as well as theoretical models are needed to estimate *in situ* exposure.

Experimental techniques are being explored to provide calibration that more closely reflects tissue propagation [1, 18]. Lossy fluids such as castor oil and Dow Corning 710 [23] may provide more useful information since they possess acoustic properties closer to tissue than water. However, these media are difficult to work with and possess attenuation quadradically related to frequency, whereas soft tissue has been shown to be almost linearly dependent with frequency. Preston et al. have taken an experimental approach to predict *in situ* exposure by inserting an acoustical attenuator in the ultrasound field between the transducer and hydrophone to mimic the path [18]. To compare and validate different techniques, effective mathematical models are needed to deal with the propagation of finite amplitude waves.

Theoretical models are useful to calculate fields resulting from nonlinear wave propagation. The specific goal of this thesis is to compare axial fields using the FDA linear derating scheme with nonlinear propagation in tissue medium. This is accomplished by first generating a nonlinear field in water and subsequently applying FDA linear derating to the first three frequency components. These derated fields are then compared to a nonlinear wave generated using lossy tissue parameters. This procedure is repeated at different source acoustic pressures to track the growth of harmonics in water and tissue media.

Some basic principles of ultrasound are first presented in Chapter 2 along with motivation to describe accurately the acoustic fields since high amplitude acoustic fields may induce biological damage. Chapter 3 introduces nonlinear propagation under lossless conditions. The discussion is subsequently extended to include thermoviscous losses which will be shown to play a significant role on the fields generated in water and tissue.

The theoretical model used to generate the nonlinear fields is the Khoklov-Zaboletskaya-Kuznetsov (KZK) equation. The numerical solution developed by Aanonsen [3] has been shown to accurately describe the fields near the beam axis and is briefly described in Chapter 4. The simulation results comparing the FDA derating criterion and the nonlinear fields generated using lossy tissue parameters are presented in Chapter 5. The overall goal is to provide some insights of the role of current calibration procedures and relate them to the simulated fields in lossy media which resemble actual fields.

# CHAPTER 2
# ULTRASONIC EXPOSURE

Ultrasound is the branch of acoustics at frequencies above the range of audible sound. Applications of this field are used extensively in sonar, nondestructive evaluation, and, of interest here, medical technology [16]. The basic operating principles of ultrasound are briefly presented in this chapter. The interaction of sound within tissue is also discussed since high intensities and prolonged exposure may result in biological damage. As a result, measurement guidelines have been established to provide exposure information [1, 20, 21].

## 2.1 Principles of Ultrasound

Acoustic waves are particle displacements in a medium due to a pressure disturbance. As the wave propagates, the fluid particles oscillate about the equilibrium point. Ultrasonic waves are generated by converting electrical energy into acoustic energy through the application of a piezoelectric material. This mechanical structure will resonate at a range of frequencies when a disturbance impinges on its surface converting acoustic signals into electrical energy. Diagnostic imaging systems use this principle to transmit and receive acoustic waves that constitute a pulse-echo system [22]. A pulsed signal is usually emitted into the body using a transducer. A portion of the energy is reflected back when a scattering structure or an interface with a different impedance is encountered. The return signal is received with the same transducer where the mechanical energy is now converted into electrical energy. This echo signal is subsequently processed to yield an A-line representing scattering strength as a function of time or depth This procedure is repeated for different scan directions by steering of the beam such that the A-lines at different positions form a composite two-dimensional image.

Modern imaging systems typically employ a number of transducer elements to increase the resolution in the lateral direction and electronically steer the beam. However, a

circular plane piston transducer provides a basic understanding of linear and nonlinear wave propagation. The radiated field can be divided into the two regions as shown in Figure 2.1. The Fresnel zone or the near-field is characterized by a well-collimated sound beam where the wave fronts are approximated as plane waves [16] since beam spreading is not appreciable for a plane piston transducer. This region also contains strong interference as exhibited by the spatial oscillations along the beam axis in Figure 2.2. The region beyond the last axial maximum is given by the transition distance, $a^2/\lambda$, is the called the Fraunhofer zone or the far-field where the phase fronts are described by spherical spreading. The acoustic pressure amplitude along the beam axis as a result decays with a 1/x dependence where x is the axial distance from the transducer.

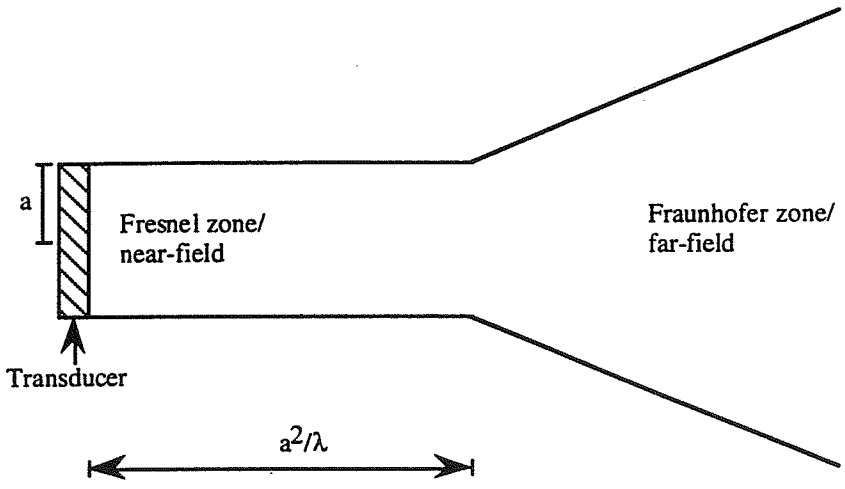


Figure 2.1: Near/far-field regions of a plane piston transducer where $a^2/\lambda$ represents the transition distance [10].

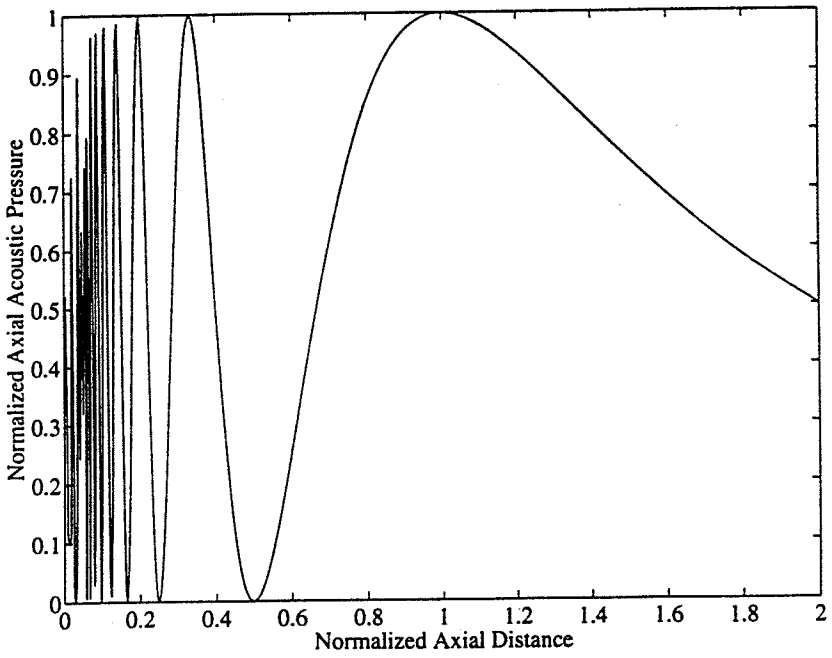


Figure 2.2: Normalized axial acoustic amplitude pressure for a plane piston transducer with a radius 1.0 cm and frequency of 5.0 MHz. The axial distance is normalized by the Fresnel length, $a^2/\lambda$.

As a wave propagates, acoustic energy is attenuated due to scattering and absorption. However, scattering comprises a very small portion of the energy lost in a homogeneous medium whereas absorption accounts for about 95% through thermal processes [19]. The acoustic pressure amplitude of the wave decreases exponentially as a function of distance. For example, given a monochromatic wave with peak acoustic pressure amplitude at the source, $p_s$, the resulting pressure waveform in the direction of the propagation, x, is given by

$$p(x) = p_s e^{-\alpha x} e^{j(\omega t - kx)} \tag{2.1}$$

where $\alpha$ is the attenuation coefficient for the medium, t is time, and k (=$\omega$/c) is the propagation constant [10] with the angular frequency, $\omega$, and the speed of sound, c. Figure 2.3 shows the effect of attenuation on the acoustic pressure amplitude along the beam axis for

a wave emitted by a plane piston transducer. Attenuation due to absorption mechanisms will be discussed in greater detail in the next chapter as it pertains to nonlinear wave propagation.

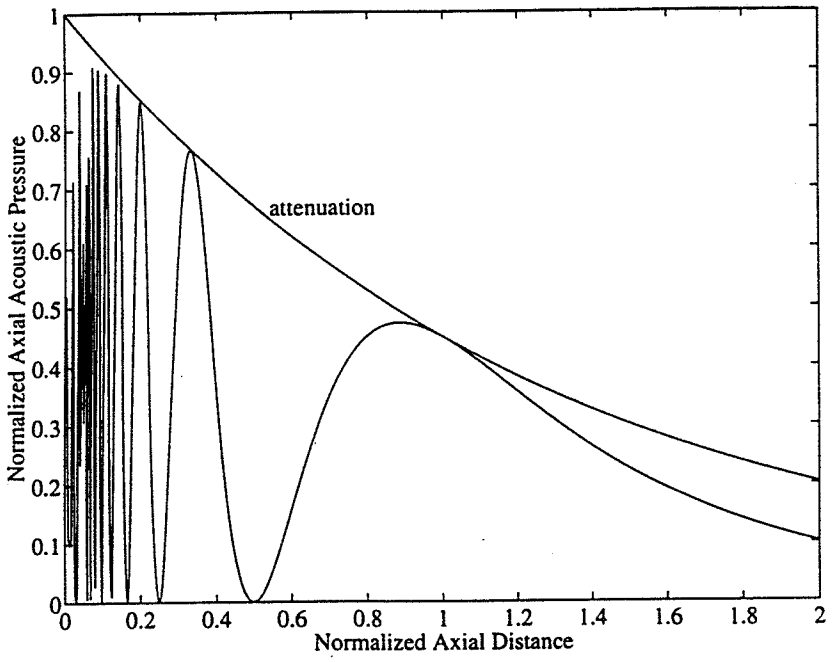


Figure 2.3: The effect of attenuation on the axial acoustic pressure field of Figure 2.2. The attenuation factor is given by $\exp(-\alpha x)$ where $\alpha = 0.8$ Np/cm.

## 2.2 Biological Effects

Ultrasound has become a widely used diagnostic tool within the medical community for blood flow analysis, detection of cancerous cells, fetal imaging, and even lithotripsy for treatment of kidney stones. The interaction of ultrasonic waves with tissue is a complicated phenomenon. As a result, numerous experiments have been performed to monitor the levels at which biological damage is induced. Some of the known mechanisms producing bioeffects are cavitation, streaming, and thermal effects [1].

Cavitation is the interaction of small gaseous bodies with tissue where the bubbles begin to oscillate in the presence of an acoustic field [1]. When the amplitude of the oscillations exceeds the radius of the bubble at resonance, the bubble will collapse, causing an inrush of fluid. It has been reported that these sudden implosions give rise to high temperatures near the surface of the bubble [1]. Another mechanism closely associated with cavitation is streaming in which the propagation of high amplitude sound waves around an oscillating bubble creates eddy currents which are hypothesized to cause shearing against the tissue wall [1]. Lesions have been produced in cat brains under continuous wave conditions at 3 MHz and pressures of 8 MPa [1]. Commercial scanning equipment also has the capability to produce lung hemorrhaging in adult mice [1]. Although biophysical damage resulting from bubbles have been observed in laboratory animals, similar effects have not been confirmed in humans.

Localized heating as a result of ultrasonic absorption has been the focus of extensive research [1, 19, 20]. The optimal temperature for normal mammalian cells is 37°C where temperature elevation increases the rate of enzymatic activity [17]. At temperatures exceeding 45°C, these biochemical processes decrease and may cease, resulting in coagulation of protein and eventually cell damage [1]. It has been observed from rats to primates that high temperature and high exposure times can result in malformations in newborns.

The bio-heat transfer equation is often employed to characterize local tissue heating [19]. The resulting temperature rise in tissue is dependent on the acoustic beam profile and the characteristics of the medium such as absorption, heat conduction, and perfusion. A typical heating pattern associated in the near-field of a plane piston transducer is shown in Figure 2.4 for a 2.25 MHz unfocused transducer [19].

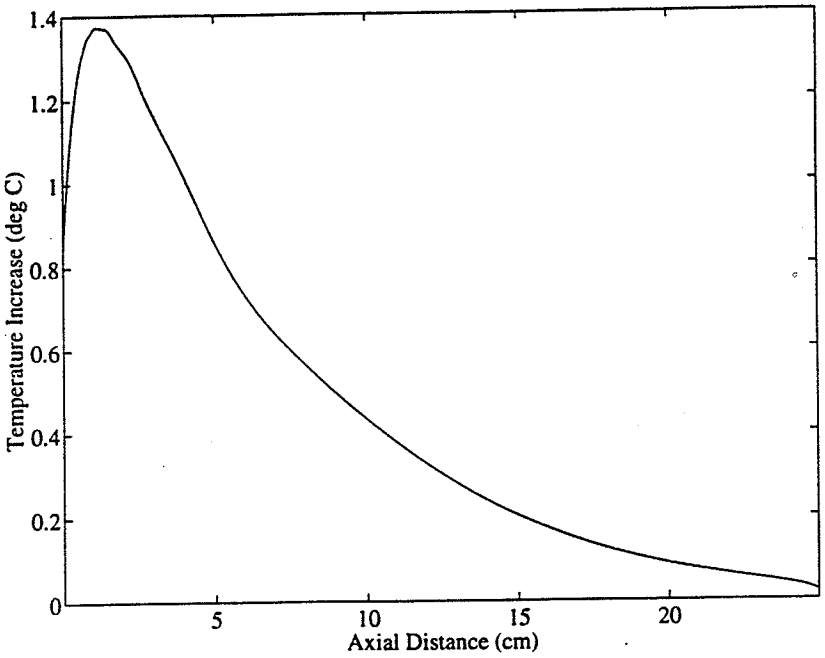


Figure 2.4: Typical heating pattern generated using the bio-heat equation for water medium from an unfocused transducer with radius of 1.0 cm operating at 2.25 MHz with an acoustic pressure of 500 kPa.

## 2.3 Output Labeling

The Food and Drug Administration (FDA) has developed guidelines on the maximum allowable output fields that can be produced *in situ* by ultrasonic equipment. The next generation of diagnostic equipment has the capabilities to produce significantly higher output levels. As a result, the FDA along with professional societies such as the American Institute of Ultrasound in Medicine (AIUM) has developed output display guidelines that provide the clinician information in terms of thermal and mechanical indices regarding exposure levels employed for different modes of operation [20].

A basic quantity for all measurements that describes the amount of energy present is the time average intensity. Intensity is the average rate of flow of energy per unit area as defined by

$$I = \frac{1}{T}\int_0^T pudt = \langle pu \rangle_t \tag{2.2}$$

where T is the period of the temporal waveform [10]. For plane waves, the acoustic pressure and particle velocity are related by the characteristic acoustic impedance, ρc, so that Equation (2.2) can be rewritten in terms of a single variable

$$I = \frac{p_0^{\,2}}{2\rho c}. \tag{2.3}$$

For continuous waves of a single frequency, this quantity is also referred to as the temporal average intensity ($I_{ta}$) whereas for discrete operating modes, the intensity is given in terms of an integral of the temporal waveform. The relevant parameters for a typical temporal waveform are the compressional pressure ($p_c$) and the rarefactional pressure ($p_r$) which represent the positive and negative peak acoustic pressures, respectively.

As shown earlier in Figure 2.2, the acoustic pressure fields vary with spatial position and attenuation. However, only the *in situ* global maximum is specified in the output labels which are denoted by $I_{spta.3}$. The ".3" in the subscript is a derating factor of 0.3 dB/cm-MHz that represents the estimate of acoustic fields in lossy media such as soft tissue.

Another measurement index has been devised to give a better indication of the likelihood of nonthermal bioeffects such as cavitation. The mechanical index (MI) is given by

$$MI = \frac{p_{r.3}}{\sqrt{f}} \tag{2.4}$$

where $p_{r.3}$ is the derated peak compressional pressure given in MPa and f is frequency in MHz. Similarly, the thermal index (TI) is the ratio of total acoustic power to the power required to raise the temperature of the medium by 1°C [20]. This index alerts the clinicain regarding the potential for significant temperature rise during scanning. As higher output levels are achieved, accurate characterization of the acoustic fields in tissue is necessary to avoid any potential hazards to patients.

### 2.4 Tissue Derating

Acoustic output labels by manufacturers are specified in terms of *in situ* values to provide an indication of output levels for tissue where the maximum allowable $I_{spta.3}$ is 720 $mW/cm^2$ [20]. However, all calibration measurements are made in water. To obtain an estimate of acoustic quantities representative of typical low loss tissue, a derating factor of 0.3 dB/cm-MHz is subsequently applied. However, this estimate is based on a linear propagation model which means that if the transducer output power is doubled, then the field intensity will also increase by a factor of two. The AIUM bioeffects committee issued the following statement regarding the role of output labeling of diagnostic equipment [1]:

> Existing tissue models that are based on linear propagation may underestimate acoustical exposures when significant saturation due to nonlinear distortion of beams in water is present during the output measurement.

The use of a linear propagation model may not be valid for high amplitudes in the presence of nonlinear, thermoviscous wave propagation which may include saturation. This means that at sufficiently high amplitudes used in diagnostic ultrasound, increasing power to the transducer may not increase the measured output fields in a 1-1 ratio but simply result in transfer of energy to the higher harmonic frequencies leading to greater frequency-dependent

absorption in the medium which may lead to inaccurate reporting of predicted *in situ* exposure levels. To provide a basic understanding, the acoustic pressure is investigated since this is the primary measured quantity upon which intensity and the mechanical and thermal indices are based.

# CHAPTER 3
# NONLINEAR WAVE PROPAGATION

Linear acoustics deals with the ideal case of sound waves of infinitesimal amplitude. However, when the amplitude of the wave becomes sufficiently large, nonlinear processes such as harmonic distortion are observed. This chapter provides a basic understanding of waveform distortion produced in a fluid medium under lossless conditions. The properties of the medium are included through the Navier-Stokes equations [12] to account for the thermoviscous losses due to attenuation and heat conduction.

## 3.1 Nonlinear Processes

The equations of motion are necessary to describe acoustic wave propagation in a fluid since the fluid particles must obey physical laws. First, a continuity equation is needed to describe the conservation of mass through a fixed volume. A second equation attributed to Euler is simply a force balance equation that follows from Newton's second law for a specified mass of a fluid. Finally, the equation of state relates the internal restoring force of a fluid subject to a deformation from an acoustic disturbance. The simplified continuity equation, Euler's equation, and the equation of state with diffraction and dissipation neglected are as follows [10]:

$$\frac{\partial \rho}{\partial t} + \frac{\partial (\rho u)}{\partial x} = 0 \tag{3.1}$$

$$\rho \frac{Du}{Dt} + \frac{\partial p}{\partial x} = 0 \tag{3.2}$$

$$\frac{Du}{Dt} = \frac{\partial u}{\partial t} + u\frac{\partial u}{\partial x}$$

$$p = p(\rho) \tag{3.3}$$

where p is the total pressure, $\rho$ is the total density, u is the particle velocity while t is the time coordinate and x is the spatial coordinate in the direction of propagation, respectively. These equations are inherently nonlinear where the physical sources of nonlinearity are attributed to convection and the pressure-density relationship which result in gradients between fluid particles. In the ideal case, perturbations around the equilibrium point are small so that the pressure and density were related by a constant. However, such an approximation is no longer valid for finite amplitude waves where quadratic terms must be included in the theoretical development. We begin by performing a Taylor series expansion on the equation of state

$$p = p_0 + \left[\left(\frac{\partial p}{\partial \rho}\right)_s\right]_{\rho=\rho_0} (\rho - \rho_0) + \left[\left(\frac{\partial^2 p}{\partial \rho^2}\right)_s\right]_{\rho=\rho_0} \frac{(\rho - \rho_0)^2}{2} + \ldots \tag{3.4}$$

where $p_0$ and $\rho_0$ are the ambient pressure and density in the fluid, respectively, and s is the entropy per unit mass. Assuming constant entropy, Equation (3.4) is rewritten as [16]

$$p - p_0 = A\left(\frac{\rho - \rho_0}{\rho_0}\right) + \frac{B}{2}\left(\frac{\rho - \rho_0}{\rho_0}\right)^2 + \ldots \tag{3.5}$$

where the coefficients A and B are defined as

$$A = \left[\rho_0 \left(\frac{\partial p}{\partial \rho}\right)_s\right]_{\rho=\rho_0}$$

$$B = \left[\rho_0^{\,2} \left(\frac{\partial^2 p}{\partial \rho^2}\right)_s\right]_{\rho=\rho_0}$$

and the ratio of B/A is the nonlinearity parameter. Retaining up to the quadratic term in Equation (3.5), a second-order description relating density and pressure is obtained

$$\frac{dp}{d\rho} = \frac{A}{\rho_0} + B\frac{\rho}{\rho_0^2} = c_0\left(1 + \frac{B}{A}\frac{u}{c_0}\right) \tag{3.6a}$$

where the following substitutions have been made:

$$p = c_0^2\rho \text{ with } c_0^2 = \frac{dp}{d\rho}u \tag{3.6b}$$

$$\frac{p}{u} = \rho_0 c \ . \tag{3.6c}$$

Equation (3.6a) is borrowed from linear acoustics which is the pressure-density relation to the first order with $c_0$, the speed of sound at infinitesimal amplitude. The latter expression is the characteristic equation describing the impedance for plane wave propagation.

The speed of propagation due to a finite disturbance is, in fact, not spatially uniform for all points but depends on the local particle velocity, u. As a result, the general expression that describes a plane wave propagating in lossless media is described by the following:

$$\frac{dx}{dt} = u(x) + c \tag{3.7}$$

and when combined with Equations (3.6), yields the fundamental relationship governing nonlinear acoustics:

$$\frac{dx}{dt} = c_0 + \beta u(x) \tag{3.8}$$

where $\beta = \left(1 + \frac{B}{2A}\right)$ is the nonlinearity coefficient of the medium.

For an initially sinusoidal wave with a peak particle velocity magnitude, $u_p$, the propagation speed as a function of distance is shown in Figure 3.1 where the positive region travels faster than the negative half-cycle. As the particle velocity varies, compressional and rarefactional regions are formed, i.e., $dx/dt > c_o$ when $u > 0$ and $dx/dt < co$ when $u < 0$. At the point where the particle velocity reaches its maximum amplitude, $u = u_p$, the propagation

speed is also a maximum with $c = c_o + \beta u_p$. The trough is formed, $u = -u_p$ yielding a minimum propagation speed of $c = c_o - \beta u_p$. At points at which there is zero compression, the propagation speed is simply $c_o$ which is the infinitesimal amplitude sound speed.

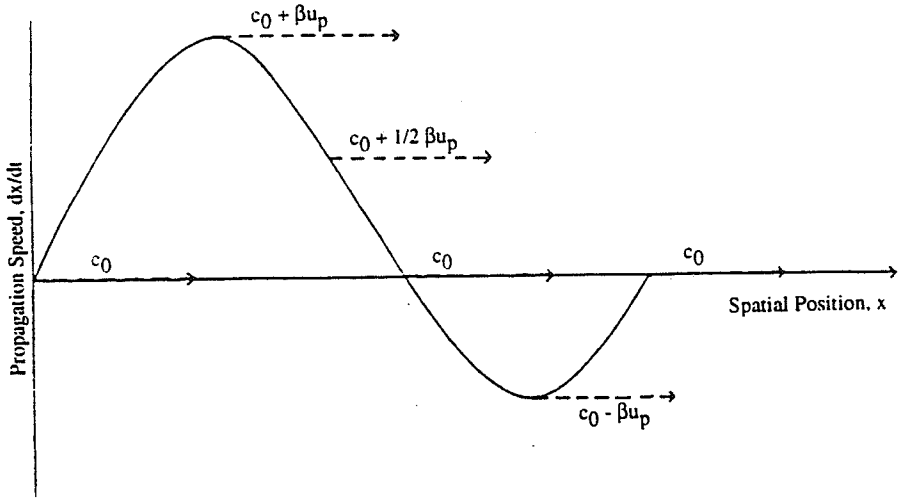


Figure 3.1: Wave distortion produced by nonuniform propagation where $u_p$ represents the peak particle velocity [8].

As a consequence of the nonuniform sound speed, the time wave profile will distort as illustrated in Figure 3.2. As the disturbance moves further away from the source, the peak in the time waveform of Figure 3.2(c) will eventually catch up with the trough forming a shock wave and subsequently a breaking wave. However, multivalued functions are physically unrealistic since they corresponds to three values of particle velocity for a single point x. That is, each spatial position and time (x,t) must uniquely determine particle velocity, acoustic pressure, and density (u, p, $\rho$) for a wave to exist. The distance at which a discontinuity is first observed is the shock formation distance, $\ell_d$, which occurs when the slope of the leading edge becomes infinite. As a result, the shock distance is

$$\ell_d = \frac{c_0^2}{\left(1+\frac{B}{2A}\right)\omega u_0}. \tag{3.9}$$

As mentioned, a multivalued function is impossible. However, loss mechanisms of the medium exist to prevent further distortion near the discontinuity. As a result, dissipative processes must be included to describe nonlinear wave propagation in fluid.

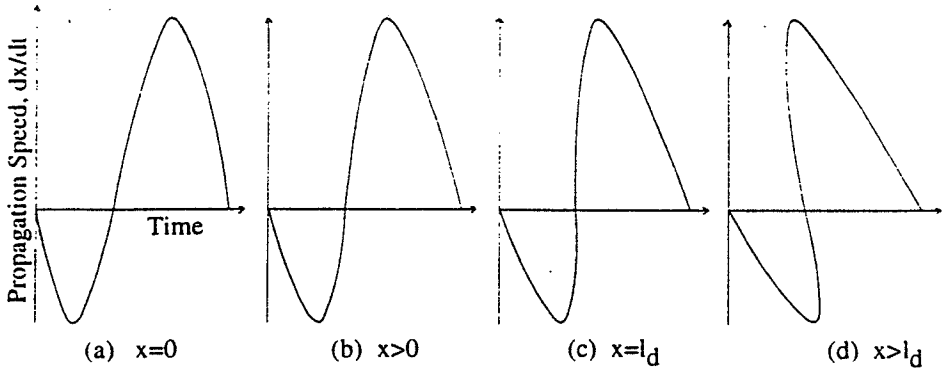


Figure 3.2: Formation of a shock leading to a multivalued wave in the absence of dissipative forces [8].

### 3.2 Dissipation

Thus far in this chapter, dissipation has been ignored. As an acoustic wave propagates, the acoustic pressure decreases with the distance traveled. Although attenuation is, in part, due to scattering, the predominant mechanism for the transfer of energy to the medium is in the form of heat. The primary mechanisms responsible for thermal dissipation are classical causes such as viscosity and heat conduction and the nonclassical causes of thermal and structural relaxation [10].

Viscosity is a frictional loss that is attributed to the relative motion of adjacent fluid particles. Shear viscosity is a measure of diffusion of momentum by molecules of higher velocities to regions having lower velocities. However, bulk viscosity is the mechanical energy lost due to compression or dilatation as the wave propagates and is, therefore, dependent on frequency. The attenuation for a plane waves due to viscosity becomes

$$\alpha_{viscosity} = \left(\frac{4}{3}\eta_s + \eta_b\right)\nabla^2 u \tag{3.10}$$

where $\eta_s$ and $\eta_b$ are the coefficients for shear and bulk viscosities, respectively [13].

Heat conduction is another classical mechanism which is attributed to fluctuations in pressure that are not in thermodynamic equilibrium. As a result, temperature gradients between the compressional and rarefactional portions of the waveform cause energy flow from the hotter to the colder regions. The attenuation from heat conduction is given by

$$\alpha_{thermal} = (\gamma - 1)\frac{\kappa}{c_p}|ku|^2 \tag{3.11}$$

where $\kappa$ is the thermal conductivity and $\gamma = c_p/c_o$ is the ratio of specific heats [13].

Thermal relaxation is a nonclassical mechanism which represents losses due to the rotational and vibrational motion of molecules in the presence of an acoustic disturbance. However, thermal relaxation does not completely account for absorption for polar liquids such as water. It has been demonstrated that thermal absorption vanishes near 4°C whereas the overall absorption is not zero [10]. Instead, the excess absorption in water is attributed to structural relaxation which results from the change in volume of the fluid rather than the change in temperature.

The combined effect of the thermoviscous losses results in frequency-dependent attenuation. For water, the attenuation increases with frequency squared for each unit distance traveled while tissue has substantially greater loss but is only linearly related with frequency.

In the description of nonlinear wave propagation, it was shown that a multivalued function results in the absence of dissipative forces for finite amplitudes. Since this is not possible for ultrasonic waves, Euler's force expression no longer accurately describes the thermodynamic properties of the medium. Instead, Equation (3.2) is replaced with the Navier-Stokes equation and the heat transport equation given by Equations (3.12) and (3.13), respectively,

$$\rho\frac{du}{dt} = -\nabla p + \left(\frac{4}{3}\eta_s + \eta_b\right)\nabla^2 u \tag{3.12}$$

$$\frac{dp}{dt} = c^2\frac{d\rho}{dt} + \left(\kappa\frac{\gamma-1}{\gamma} + \Re\right)\frac{d^2\rho}{dt^2} \tag{3.13}$$

where $\Re$ is the relaxation [13]. The Navier-Stokes equation is the equation of motion which includes viscosity, heat conduction and thermal relaxation to describe the loss of acoustic energy in the medium. Equations (3.1), (3.12), and (3.13) are the governing equations of nonlinear, thermoviscous wave propagation which will be used throughout this thesis.

### 3.3 Stages of Propagation

An example of waveform distortion in a nonlinear, thermoviscous medium at various distances from the source is given in Figure 3.3. An initially sinusoidal, high amplitude wave is emitted at the source and shown in Figure 3.3(a). As the wave propagates away from the source, distortion becomes noticeable, and a shock is formed as seen in Figure 3.3(c). The wave continues to steepen as the shock amplitude grows, and eventually the wave becomes a sawtooth (Figure 3.3(e)). Further from the source, the wave begins to weaken where the thermoviscous effects predominate due to an increase in the pressure gradients at the shock front. The frequency-dependent absorption damps out the higher components at a faster rate

returning the wave to its harmonic form but at a significantly reduced amplitude. In the old age region of Figure 3.3(h), the wave is considered to be linear with infinitesimal amplitude so that the principles of linear acoustics can be applied.

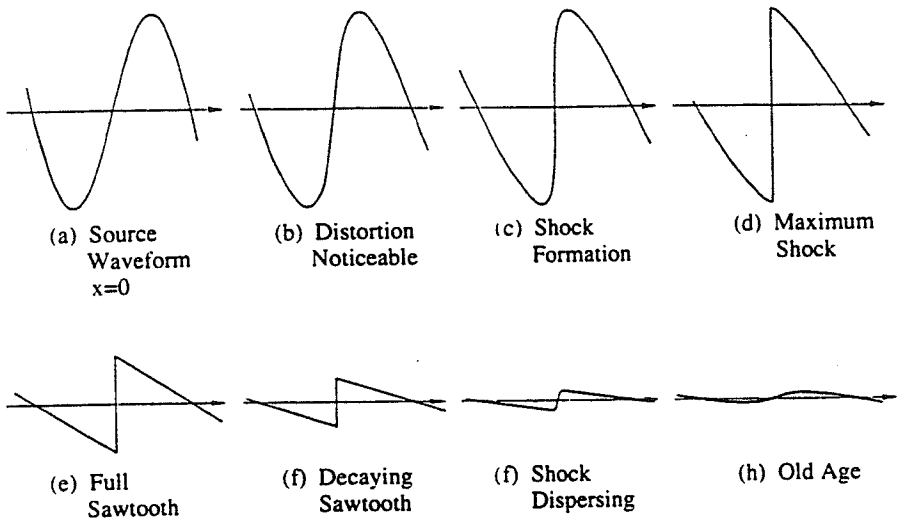


Figure 3.3: The evolution of an initially sinusoidal wave in a nonlinear, thermoviscous medium [8].

The severity of waveform distortion depends on a number of factors such as the amplitude of the transmitted wave and the nonlinearity of the medium, whereas thermoviscous losses dampen the generation of harmonics. The relative strength of distortion is, therefore, expressed by Goldberg's number [6] given by the following ratio:

$$\Gamma = \frac{1}{\alpha \ell_d} \quad . \tag{3.14}$$

The discontinuity distance, $\ell_d$, as defined previously in Equation (3.9) depends on the nonlinearity parameter and source amplitude. The discontinuity distance and dissipative

forces are viewed as competing entities since $\Gamma >> 1$ signifies that nonlinear distortion dominates with a fast rate of growth of harmonics. However, when $\Gamma << 1$ finite amplitude effects will not be appreciable since dissipative forces attenuate faster than the generation of the frequency components.

Nonlinear acoustic wave propagation has been thus far described in the time domain. However, it is often convenient to represent the acoustic pressure in the frequency domain. As a sinusoidal wave with frequency $f_o$ begins to distort, harmonic frequencies are generated at multiples of $f_o$ as shown in Figure 3.4. Just as harmonics are generated due to nonlinearity of the medium, they are also attenuated due to absorption. Since attenuation in fluid is frequency dependent, the higher harmonic pressure amplitudes are damped-out at faster rates.

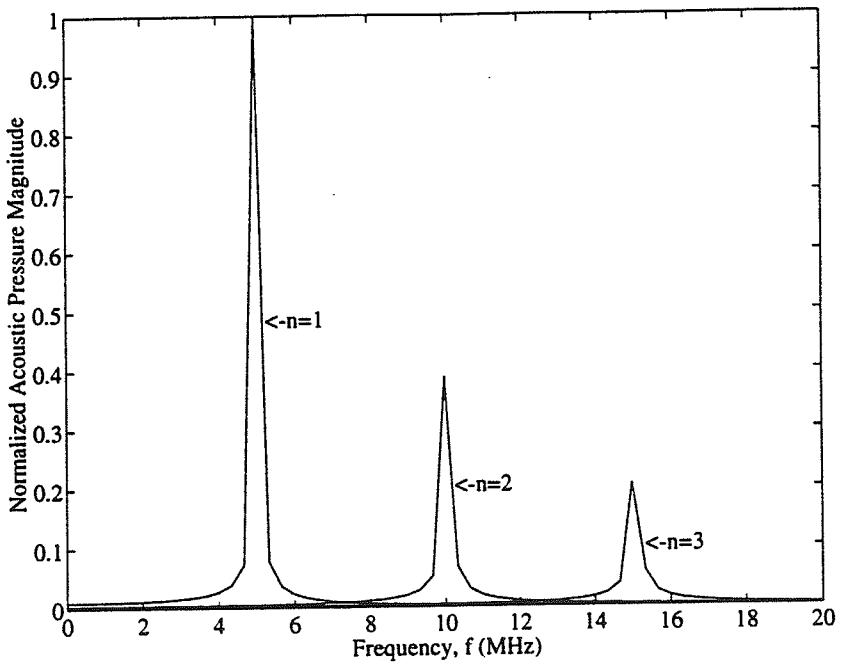


Figure 3.4: The frequency spectrum of an initially sinusoidal wave of frequency $f_o = 5$ MHz. The fundamental is shown at 5 MHz (n=1) along with its second and third harmonics at 10 (n=2), and 15 MHZ (n=3).

### 3.4 Models

The classical treatment of nonlinear wave propagation in thermoviscous media was developed by Blackstock [6]. A nonlinear wave equation was derived using the Navier-Stokes formulation. The resulting Burgers' equation [6] has been solved exactly using a nonlinear transformation. Typically, spectral solutions are obtained by asymptotic techniques where the Fubini solution [7] tracks the growth of harmonics in the near-field while Fay's solution [7] shows the subsequent decay in the far zone where dissipative forces predominate. Haran and Cook [9] derived an algorithm using the Burgers' approach for plane waves in nonlinear, lossy, nondispersive media and calculated the amount of distortion for various biological media.

With a concern for safety, accurate models are needed to describe the acoustic output in the near-field through the transition region. A nonlinear wave equation is also needed to account for diffraction due to the discontinuities along the outer rim of a plane piston transducer. Recent investigations by Christopher and Parker [14] include a Burgers' model but with the addition of a diffraction operator using a Hankel Transform.

The approach taken in this thesis is to apply the well-studied KZK model [12] in which the equation of state is expanded to the second order and thermoviscous loss terms are subsequently linearized.

# CHAPTER 4
# THE KZK EQUATION

This chapter presents a brief description of the Khokhlov-Zabolotskaya-Kuznetsov (KZK) equation [11] used to describe the pressure fields due to nonlinear, thermoviscous, diffractive wave propagation. The KZK equation is derived under the parabolic approximation which provides a reliable description in proximity to the acoustic axis. The numerical solution to the KZK that is often employed was developed by Aanonsen [3] to compute the near-field of a plane piston circular transducer. Subsequently, Baker et al. [4] experimentally verified that this model can accurately predict the near-field in a water medium at diagnostic frequencies. For a more complete discussion on the numerical derivation of the KZK equation, the reader is referred to References [2,3].

## 4.1 KZK Equation

The nonlinear wave model that accounts for nonlinearities and dissipation while including diffraction is as follows [2]:

$$\nabla^2 p - \frac{1}{c_o^2}\frac{\partial^2 p}{\partial t^2} + \frac{D}{\rho_o c_o^4}\frac{\partial^3 p}{\partial t^2} = -\frac{\beta}{\rho_o c_o^4}\frac{\partial^2 p^2}{\partial t^2}, \tag{4.1}$$

where p is the acoustic pressure, $\nabla^2$ is the Laplace operator, and t is the time. The medium is characterized by $c_o$, $\rho_o$, D, and $\beta$ which are the speed of sound for the small amplitude case, density, dissipation factor, and a parameter which includes nonlinearity, respectively. In the development of the KZK equation, several assumptions were made. For instance, a slowly changing wave profile is assumed such that the wave must travel several wavelengths from the source before distortion is appreciable. Furthermore, the wave components transverse to

the direction of propagation are small such that a parabolic approximation is applied to the well-collimated beam near the acoustic axis [11]. The resulting KZK equation in dimensionless form is [2]

$$\frac{\partial^2 P}{\partial\tau\partial\sigma} - \frac{1}{4}\nabla_\perp^2 P - \alpha r_o \frac{\partial^3 P}{\partial\tau^3} = \frac{r_o}{2l_d}\frac{\partial^2 P^2}{\partial\tau^2} \tag{4.2}$$

where scaling has been introduced so that $\tau = \omega t - kz$ is the retarded time and $\sigma = z/r_o$ is the axial propagation direction normalized by the Rayleigh distance for a periodic source [2] defined by $r_o = ka^2/2$ where a is the radius of the transducer. Additional variables are used to simplify the notation where $P = p/p_s$ is the acoustic pressure amplitude normalized by the acoustic pressure of the source, $\alpha = \frac{D\omega^2}{2\rho_o c_o^3}$ is the absorption coefficient at the frequency $\omega$, $\ell_d$ is the shock formation distance defined in Equation (3.9), and $\nabla_\perp^2$ is the Laplacian operator in the plane transverse to the direction of propagation.

### 4.2 Numerical Solution

An analytical solution to Equation (4.2) does not exist. As a result, Aanonsen [3] developed a numerical method by seeking a spectral solution having the form

$$P(u,\sigma,\tau) = \sum_{n=1}^{\infty} P_n(u,\sigma)\sin(n\tau + \Psi_n(u,\sigma))$$
$$P(u,\sigma,\tau) = \sum_{n=1}^{\infty}\{g_n(u,\sigma)\sin n\tau + h_n(u,\sigma)\cos n\tau\} \tag{4.3}$$

where u is the radial coordinate transverse to the direction of propagation while $P_n$ and $\Psi_n$ are the normalized acoustic pressure amplitude and the phase term for the $n^{th}$ harmonic component, respectively. The Fourier coefficients are, therefore, $g_n = P_n\cos\Psi_n$ and $h_n =$

$P_n \sin\Psi_n$ . Substituting Equation (4.3) into (4.2) results in an infinite set of coupled partial differential equations relating harmonic terms $g_n$ and $h_n$.

$$\frac{\partial g_n}{\partial \sigma} = -\alpha(n) r_0 g_n + \frac{1}{4n}\left(\nabla_\perp^2 h_n\right) + \frac{n r_0}{2 l_d}\left[\frac{1}{2}\sum_{k=1}^{n-1}\left(g_k g_{n-k} - h_k h_{n-k}\right) - \sum_{p=n+1}^{\infty}\left(g_{p-n} g_p - h_{p-n} h_p\right)\right] \quad (4.4a)$$

$$\frac{\partial h_n}{\partial \sigma} = -\alpha(n) r_0 h_n + \frac{1}{4n}\left(\nabla_\perp^2 g_n\right) + \frac{n r_0}{2 l_d}\left[\frac{1}{2}\sum_{k=1}^{n-1}\left(h_k g_{n-k} - g_k h_{n-k}\right) - \sum_{p=n+1}^{\infty}\left(h_{p-n} g_p - g_{p-n} h_p\right)\right] \quad (4.4b)$$

$$n = 1, 2, \ldots \ .$$

In addition, the following substitution has been made for the transverse coordinate for the case of an axisymmetric source:

$$\nabla_\perp^2 = \frac{\partial^2}{\partial \xi^2} + \frac{1}{\xi}\frac{\partial}{\partial \xi} \quad (4.5)$$

where $\xi = u/a$ is the radial distance normalized by the transducer radius, a. The frequency dependent absorption term is expressed as

$$\alpha(n) = \alpha_0 n^b \quad (4.6)$$

where $\alpha_0$ is the attenuation at the fundamental frequency, n is the harmonic, and b is the exponential frequency dependence. Viscous fluid such as water has a quadratic dependence on frequency, b = 2 [10], while attenuation in tissue has been demonstrated to be almost linearly related with b = 1.1 to 1.5 [9].

To numerically solve Equation (4.4), the infinite series must be truncated thus only the first M harmonics are retained in the calculations resulting in a system of 2M nonlinear equations. To obtain a stable numerical solution that describes the near-field oscillations, finite difference techniques are used to perform the integration [3]. Absorption and diffraction represented by the first and second terms on right side of Equation (4.4),

respectively, are evaluated by a fully implicit method while the nonlinear terms are integrated using an explicit method.

Figure 4.1 shows the rectangular mesh for the Implicit Backward Finite Difference (IBFD) method in which the coordinate space is discretized using the following standard approximations [15]:

$$
\begin{aligned}
g_n &= g_{n,i}^{j+1} \\
\frac{\partial g_n}{\partial \sigma} &= \frac{1}{\Delta\sigma}\left(g_{n,i}^{j+1} - g_{n,i}^{j}\right) \\
\frac{\partial g_n}{\partial \xi} &= \frac{1}{2\Delta\xi}\left(g_{n,i+1}^{j+1} - g_{n,i-1}^{j+1}\right) \\
\frac{\partial^2 g_n}{\partial \xi^2} &= \frac{1}{(\Delta\xi)^2}\left(g_{n,i+1}^{j+1} - 2g_{n,i}^{j+1} + g_{n,i-1}^{j+1}\right)
\end{aligned}
\tag{4.7}
$$

where $\sigma = i\Delta\sigma$ and $\xi = j\Delta\xi$ represent the axial and transverse coordinates, respectively. In addition, $g_{n,i}^{j}$ is used to denote $g_n(\xi(i), \sigma(j))$, j is the axial step index, i is the lateral step index while $\Delta\sigma$ and $\Delta\xi$ are the axial and lateral step indices, respectively.

### 4.3 Boundary Conditions

The coefficients $g_n$ and $h_n$ for each harmonic are subsequently calculated along each axial step using the coefficients of the previous axial position. However, boundary conditions must be specified at the source transducer. For a plane piston transducer with a uniform pressure distribution, the phase of the spectral solution for the first harmonic is zero, $\Psi = 0$, while the normalized pressure amplitude is one, $P_n = 1$, with all higher harmonics initialized to zero. As a result, the Fourier coefficients of Equation (4.3) at the source boundary, $\sigma=0$ and $0 < \xi < a$, are expressed as

$$g_n(\xi,0)=\begin{cases}1, & \xi<a\\ 0, & \xi>a\end{cases}\quad \text{for } n=1, \tag{4.8}$$
$$g_n(\xi,0)=0 \quad n=2,3,... \quad \text{for all } \xi$$
$$h_n(\xi,0)=0 \quad n=1,2,... \quad \text{for all } \xi\ .$$

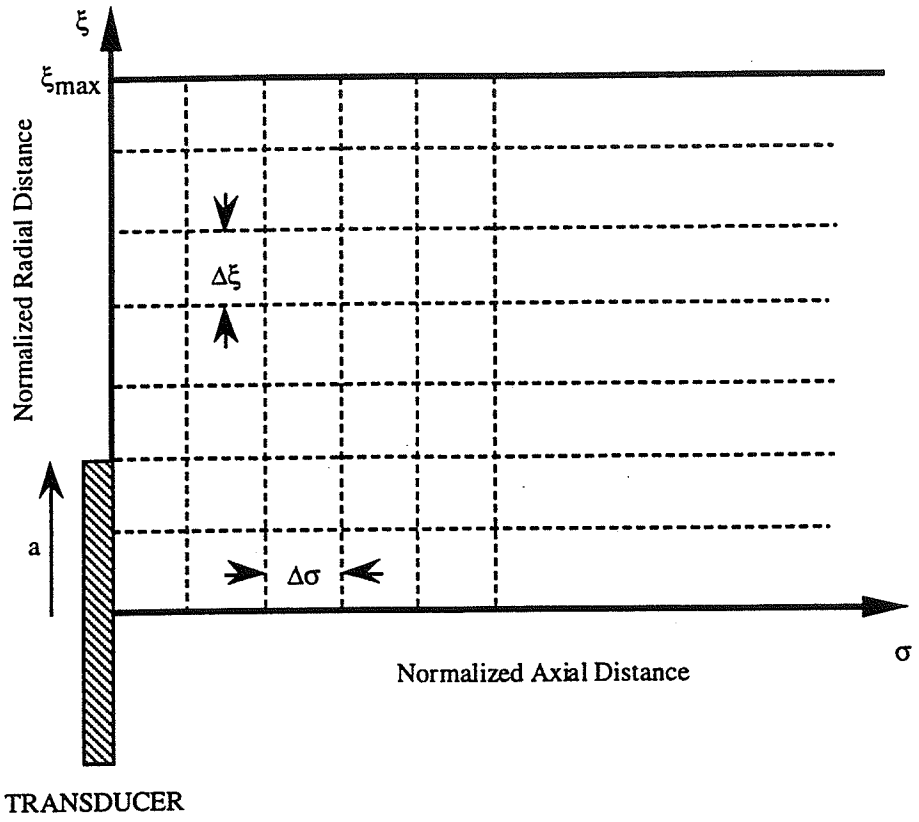


Figure 4.1: Coordinate system for the Implicit Backward Finite Difference method [9].

## 4.4 Numerical Implementation

The numerical solution to the KZK equation was implemented on a Sun SparcStation 330 using the programming language, C. The memory on this platform allowed the creation of large data arrays since the coefficients, $g_n$ and $h_n$ for each frequency along the transverse plan at an axial position were needed to calculate the coefficients at the next axial location. As the IBFD method progresses along the axial direction, the normalized acoustic pressure

amplitude with its corresponding phase for the first three harmonic components are written to output files. Furthermore, variables used throughout the programs were declared double precision to minimize errors from rounding and truncation of the data.

Numerical errors exist when implementing the solution to the KZK equation. The primary sources of these errors are attributed to the truncation of the infinite series to M harmonics. Simulations were performed by Aanonsen [3] showing effects of varying M on the axial pressure fields. In this thesis, 20 harmonics are retained in the calculations since the higher frequencies are small having a negligible contribution to the pressure amplitude.

The IBFD method is effective only when appropriate step sizes for $\Delta\sigma$ and $\Delta\xi$ are chosen in the axial and transverse directions, respectively. To guarantee stability for the iteration at each axial step, $\Delta\sigma/\Delta\xi^2 < 0.5$ is chosen. Otherwise, errors would accumulate using the iteration scheme causing the harmonic amplitudes to grow without bound. Aanonsen further calculated that with $\Delta\sigma/\Delta\xi^2 = 0.4$, the errors due to the iteration are less than $4 \times 10^{-4}$ for the normalized pressure amplitude [3]. The iteration is halted when the difference from the previous two results is less than $1 \times 10^{-4}$.

Errors also arise from limiting the maximum value for $\xi$ since a small selection would result in the acoustic beam spreading, eventually reaching this boundary. The pressure amplitude will, therefore, begin to oscillate in the transition region. As a result, an $\xi_{max} = 5.0$ allows some beam spreading through the transition region where the phase fronts are no longer well-collimated.

Step sizes of $\Delta\sigma = 2.5 \times 10^{-4}$ and $\Delta\xi = 0.025$ were selected to capture some of the oscillations in the near-field within a reasonable amount of computation time or roughly 2.5h on the SparcStation. Table 4.1 summarizes the parameters used in all of the simulations.

Table 4.1: Simulation Parameters

| | | |
|---|---|---|
| M | number of harmonics retained | 20 |
| $\Delta\sigma$ | normalized axial step size | $2.5 \times 10^{-4}$ |
| $\sigma_{max}$ | maximum axial distance | 0.75 |
| $\Delta\xi$ | normalized radial step size | 0.025 |
| $\xi_{max}$ | maximum radial distance | 5.0 |

For a more complete discussion of numerical instabilities and errors that may arise from incorrect step size selection, harmonic truncation, and integration approximations for the IBFD method, the reader is referred to References [3] and [15].

# CHAPTER 5
# SIMULATIONS

Nonlinear wave propagation is a complicated phenomenon whose behavior is dependent on the distance from the source, amplitude of the source, and acoustic properties of the medium, such as nonlinearity and attenuation. In addition, it is particularly difficult to describe the near-field oscillations attributed to interference from a plane piston transducer. As a result, simulations using the KZK model have been performed to assess the effects of the different source pressure levels on the output fields in water and tissue media. The ultrasonic fields used for this study are generated using a plane piston transducer with a radius of 19 mm transmitting a continuous wave at a single frequency of $f_0 = 2.25$ MHz.

## 5.1 Tissue Derating

Acoustic field calibrations are typically performed in water using a wideband hydrophone to measure the output pressure along the beam axis of a transducer. However, these output fields are not representative of *in situ* exposure levels since water is a low-loss medium. Tissue exposure levels are, therefore, estimated by applying a linear derating factor of 0.3 dB/cm-MHz. The objective of this section is to evaluate the validity of water calibrations to predict *in situ* exposure using the linear derating scheme prescribed by the FDA.

The KZK nonlinear wave model developed in the last chapter is utilized to generate fields in water and tissue media as per the following three-step process:

(1) KZK simulations are performed using the acoustical properties of water to mimic actual measurement conditions (**water fields**).

(2) Linear derating of the water fields is performed to mimic the FDA *in situ* field conditions (**derated fields**).

(3) KZK simulations are performed using the acoustical properties of tissue to mimic actual *in situ* field conditions (**tissue fields**).

The first step is to describe nonlinear wave propagation using the KZK model in a water medium. The acoustical properties of water for the simulations are summarized in Table 5.1 where the density, the small amplitude speed of sound, and the nonlinearity parameters are $\rho = 1000$ kg/m$^3$, $c_o = 1480$ m/s, and B/A = 5.0, respectively [16]. In addition, water is a low-loss fluid whose attenuation has a quadratic dependence on frequency with A = 0.00219 dB/cm-MHz$^2$ [10]. The attenuation coefficient in water for the simulations at the fundamental frequency, $f_o = 2.25$ MHz, is therefore 0.011 dB/cm.

Table 5.1: Simulation parameters for fields at the source frequency, $f_o = 2.25$ MHz

| | | |
|---|---|---|
| $c_o$ | speed of sound | 1480 m/s |
| $\rho$ | density | 1000 kg/m$^3$ |
| B/A | nonlinearity parameter | 5.0 |
| $A_{water}$ | attenuation in water | 0.011 dB/cm |
| $A_{derated}$ | attenuation in derated and tissue fields | 0.68 dB/cm |

The linear derating described in step (2) is now applied to the fields of step (1). The attenuation coefficients using the FDA derating criteria for the frequencies components at 2.25, 4.50, and 6.75, are 0.675, 1.35, and 2.03 dB/cm, respectively, which result in the derated axial acoustic pressure fields based on the FDA scheme. These fields are subsequently compared to the axial fields generated in step (3) with attenuation of tissue to simulate *in situ* conditions using the KZK model. The attenuation coefficient for tissue field simulations at the fundamental frequency, 2.25 MHz, is 0.68 dB/cm with the attenuation for the higher

harmonics linearly dependent on the frequency. The other acoustical parameters such as the density, speed of sound, and nonlinearity are the same as those for water such that the only variable is the source acoustic pressure $p_s$.

A comparison of the derated fields to tissue fields is accomplished by evaluating the peak acoustic pressure amplitudes of the diffractive maximum and last axial maximum occurring in the near-field and transition regions, respectively. The ratio of the peak acoustic pressure amplitudes for the derated, $p_{n,derated}$, and tissue, $p_{n,tissue}$, fields gives a measure of the comparison between the two quantities

$$p_{n,ratio} = p_{n,derated} / p_{n,tissue} \qquad n=1,2,3 \qquad (5.1)$$

where n denotes the frequency component with n=1 for the fundamental, n=2 for the second harmonic, and n=3 for the third harmonic. The acoustic pressure of the derated field underestimates the acoustic pressure of the tissue field when the ratio of Equation (5.1) is less than one ($p_{n,ratio} < 1$). Conversely, when the ratio is greater than one ($p_{n,ratio} > 1$), the acoustic pressure for the tissue fields is overestimated by the derated fields while a value of unity ($p_{n,ratio} = 1$) denotes perfect agreement between the two acoustic pressure fields being compared.

To provide some insight into the rate of attenuation between the derated fields and the tissue fields, the differences in the axial location of the peak acoustic maximum are also compared. The axial shift is calculated as follows:

$$z_{n,shift} = z_{n,tissue} - z_{n,derated} \qquad n=1,2,3 \qquad (5.2)$$

where $z_{n,tissue}$ and $z_{n,tissue}$ denote the distance of the peak acoustic pressures from the source for tissue and derated fields, respectively, at the nth harmonic.

The axial acoustic pressure field distributions throughout this chapter are presented in terms of normalized acoustic pressure amplitudes. This normalization is incorporated within the KZK simulations through the dimensionless quantity

$$P = p / p_s \tag{5.3}$$

where p is the acoustic pressure along the beam axis and $p_s$ is the acoustic pressure at the source. Therefore, P provides a direct way to evaluate the effects of varying the acoustic pressure amplitude emitted by the transducer on the growth of harmonics components along the beam axis. Three cases, $p_s$ = 25, 250, and 2500 kPa, are discussed in detail in the following sections.

### 5.1.1 Linear case, $p_s$ = 25 kPa

We start the discussion by looking at the acoustic pressure fields generated from a source transducer with a peak acoustic pressure amplitude of 25 kPa. This is referred to as the linear case since the normalized acoustic pressure amplitude of the water fields does not exhibit significant nonlinearities as shown in Figure 5.1. The acoustic pressure amplitude at the fundamental frequency of 2.25 MHz, n=1, reaches an axial peak in the transition region at a distance from the transducer face of 12.4 cm with a normalized peak acoustic pressure amplitude of 1.97. The corresponding normalized peak acoustic pressures in this region for the second and third harmonics at 4.50 (n=2) and 6.75 MHz (n=3) are 0.098 and 0.011, respectively, located 23.6 and 32.8 cm from the source. An expanded view of the second and third harmonics is provided in Figure 5.2. The degree of nonlinearity is determined by the presence of the harmonics relative to the fundamental as given by the following percentage:

$$\text{harmonic content (\%)} = P_n / P_1 * 100 \qquad n=2,3 \tag{5.4}$$

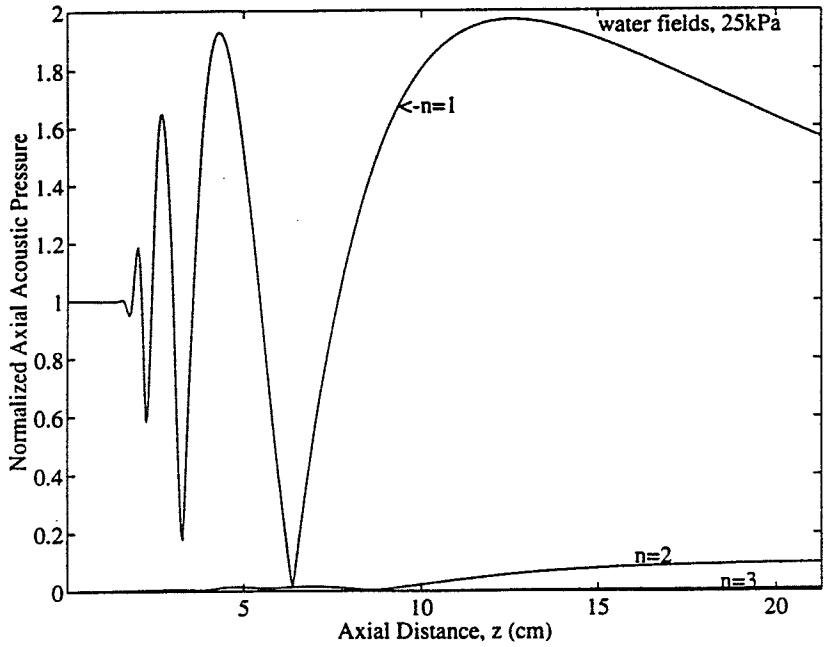


Figure 5.1: Normalized axial acoustic pressure amplitude vs. axial distance for water fields at frequencies 2.25 (n=1), 4.50 (n=2), and 6.75 MHz (n=3) when $p_s$ = 25 kPa.

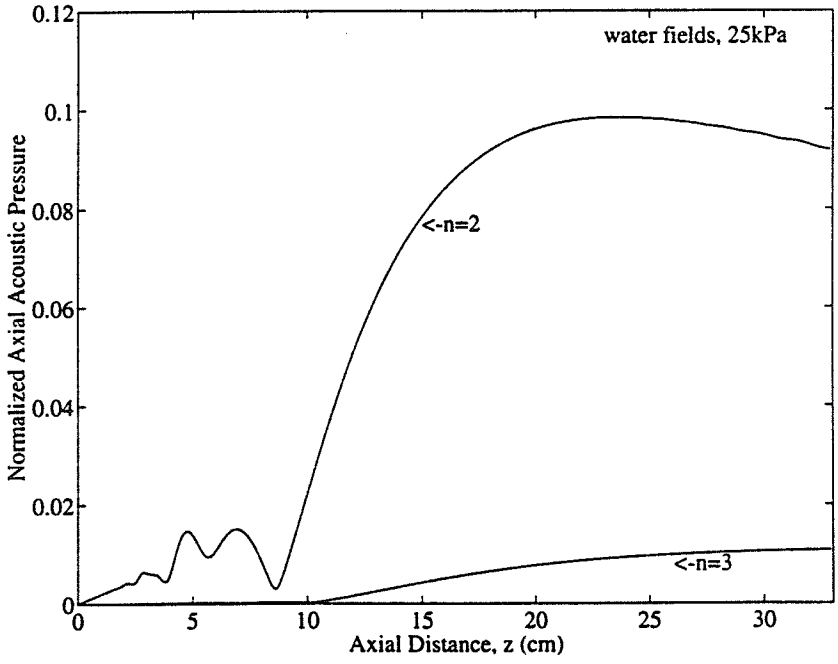


Figure 5.2: Normalized axial acoustic pressure amplitude vs. axial distance for water fields at frequencies 4.50 (n=2) and 6.75 MHz (n=3) when $p_s$ = 25 kPa.

where $P_n$ is the normalized acoustic pressure of the nth harmonic while $P_1$ is the normalized acoustic pressure of the fundamental component (n=1) at 2.25 MHz. Using this criterion, the harmonic content of frequencies at 4.50 and 6.75 MHz represent less than 5 and 0.6%, respectively, at the last axial maximum in the transition region.

The diffractive maximum in the near-field occurs 4.3 cm from the source with a normalized acoustic pressure amplitude of 1.93. The presence of the harmonics is significantly less in this region than the transition region where the peak acoustic pressure maxima are located 6.92 and 6.14 cm from the source with amplitudes of 0.015 and 0.00021, respectively, yielding harmonic contents of 1 % and 0.01%, thus demonstrating that the presence of harmonic components is not significant in water fields for $p_s$=25 kPa.

The FDA linear derating applied to the water fields yields the derated field plots of Figures 5.3 and 5.4. The derating process has reduced the peak acoustic pressure amplitudes of all frequency components. The spatial dependence of attenuation has a greater impact further away from the source so that the axial peak acoustic pressure amplitude for the fundamental frequency component occurs closer to the source than it did in the water field calculations. In addition, the higher-frequency terms at 4.50 and 6.75 MHz undergo greater reductions in the acoustic pressure amplitudes due to the frequency dependence of attenuation.

The normalized peak acoustic pressure amplitudes in the near-field for the fundamental and the second and third harmonics are 1.38, 0.0071, and 0.00064, respectively, at axial ranges of 4.26, 4.69, and 5.02 cm. The resulting harmonic content using Equation (5.4) is now 0.5 and 0.005% for n=2 and n=3, respectively. Similarly, the harmonic content in the transition region is determined. The normalized peak acoustic pressures at the last axial maxima for frequencies at 2.25, 4.50, and 6.75 MHz are 0.830, 0.0082, 0.00013, respectively, with corresponding axial ranges of 10.1, 13.2, and 14.5. The resulting harmonic content is 1% for the second harmonic and 0.05% for the third harmonic. Linear derating, as a result, decreases even further the level of harmonic presence with respect to the fundamental so that distortion along the beam axis is not appreciable.

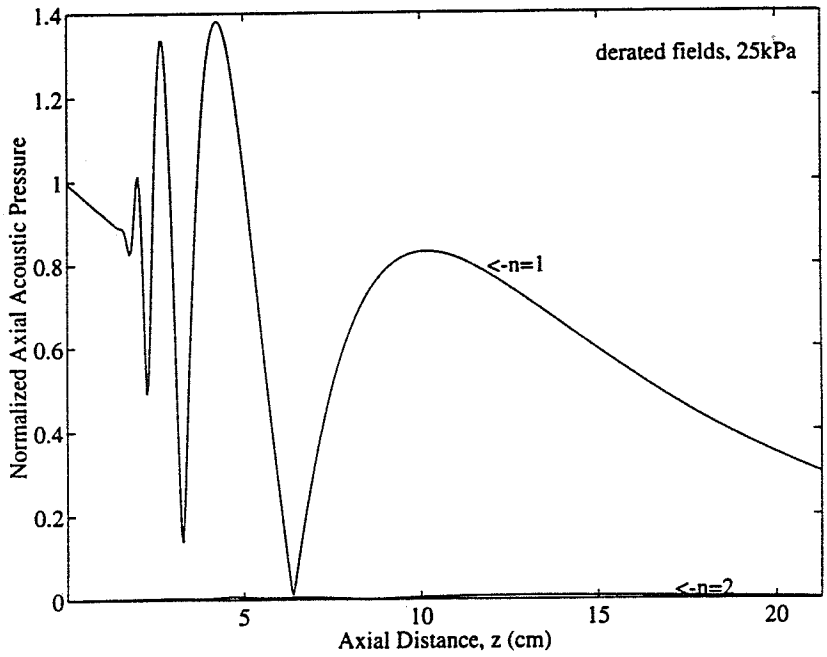


Figure 5.3: Normalized axial acoustic pressure amplitude vs. axial distance for derated fields at frequencies 2.25 (n=1) and 4.50 MHz (n=2) when $p_s$ = 25 kPa.

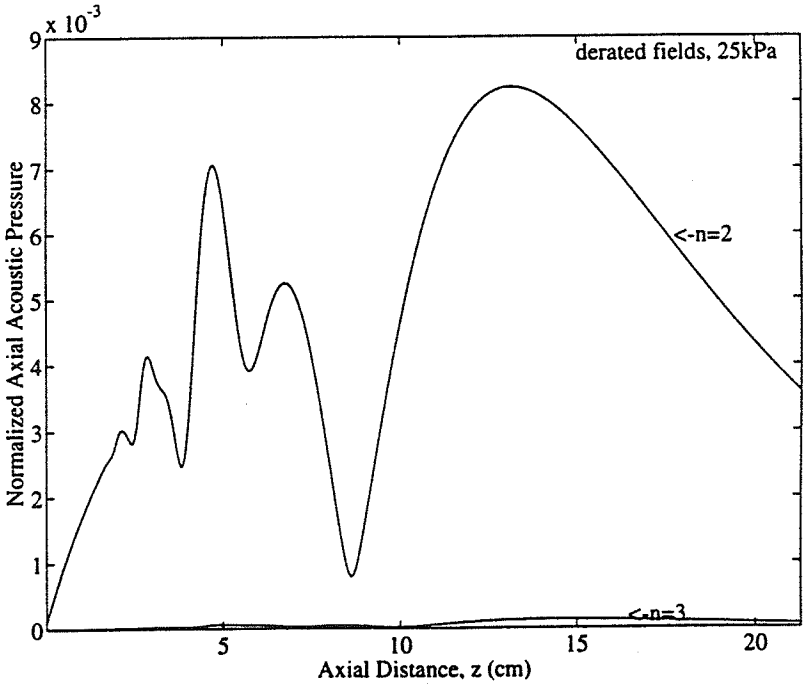


Figure 5.4: Normalized axial acoustic pressure amplitude vs. axial distance for derated fields at frequencies 4.50 (n=2) and 6.75 MHz (n=3) when $p_s$ = 25 kPa.

The tissue fields along the beam axis are observed in Figures 5.5 and 5.6 when the nonlinear model is used to generate the acoustic pressure using tissue parameters (see Table 5.1). The axial plots of the tissue fields exhibit features similar to the derated fields with the spatial peak acoustic pressure of the fundamental occurring in the near-field while spatial peaks of the second and third harmonics lie in the transition region. The normalized peak acoustic pressures, in the transition region, for the higher frequency components have amplitudes of 0.0085 and 0.00014 for 4.50 and 6.75 MHz located 13.3 and 14.6 cm from the source, respectively, while the fundamental has an amplitude of 0.837 located 10.2 cm form the source. This results in a harmonic content of 1% for n=2 and 0.02% for n=3 using Equation (5.4) which are almost identical to the derated field case.

The peak acoustic pressures of the derated fields are now compared with the respective tissue fields. The near-field and transition regions are examined based on Equations (5.1) and (5.2). The ratios of the peak acoustic pressure amplitudes, $p_{n,ratio}$, in the near-field are 0.99, 0.99, and 0.97 for frequency components at 2.25 (n=1), 4.50 (n=2), and 6.75 MHz (n=3), respectively, while the difference in the axial ranges, $z_{n,shift}$, are 0.0, 0.05, and 0.01 cm. In the transition region, $p_{n,ratio}$ are now 0.99, 0.96, 0.93 for n=1, 2, and 3, respectively, with all of the frequency components having an axial shift of 0.1 cm.

Tables 5.2 and 5.3 summarize the normalized acoustic pressures at 2.25, 4.50, and 6.75 MHz in the near-field and transition regions, respectively. The last row referred as "comparison" summarizes the results for $p_{n,ratio}$ and $z_{n,shift}$ represented by the first and second numbers of the each cell, respectively, for each frequency component. In all cases, the ratios for $p_{n,ratio}$ are 0.93 or greater while the axial shifts, $z_{n,shift}$, are 0.1 cm or less, demonstrating that for a source pressure of 25 kPa, nonlinear distortion does not show significant disparities in the two derating schemes. This is, in part, due to the low acoustic pressure of harmonics along the beam axis such that most of the energy is maintained in the fundamental frequency. As a result, nonlinear distortion does not significantly affect the estimates for *in situ* acoustic pressure amplitudes under the FDA derating scheme.

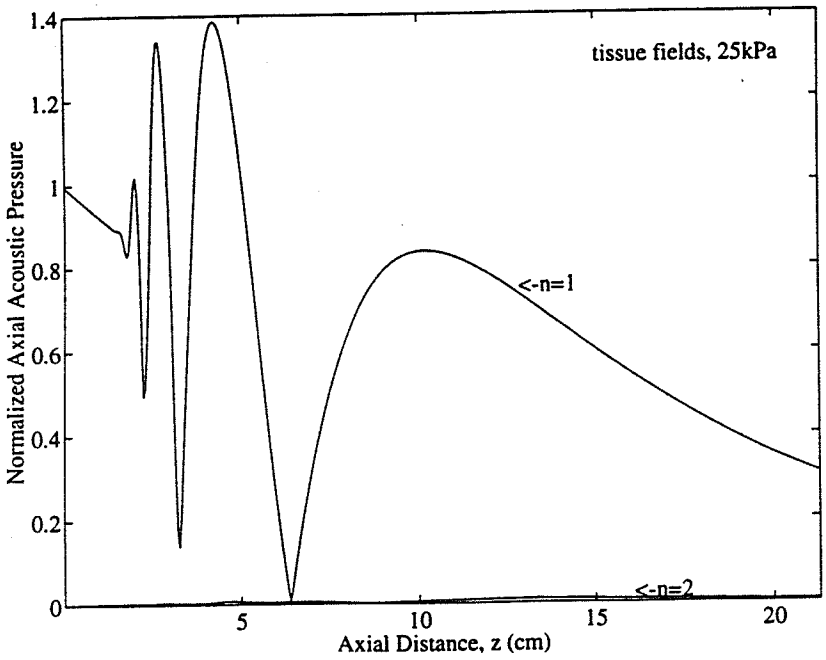


Figure 5.5: Normalized axial acoustic pressure amplitude vs. axial distance for tissue fields at frequencies 2.25 (n=1) and 4.50 MHz (n=2) when $p_s$ = 25 kPa.

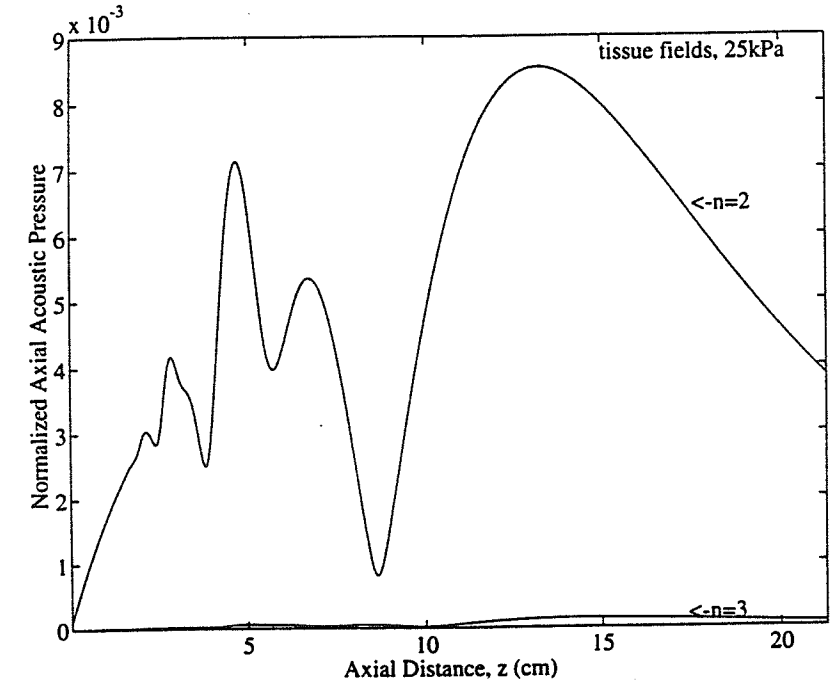


Figure 5.6: Normalized axial acoustic pressure amplitude vs. axial distance for tissue fields at frequencies 4.50 (n=2) and 6.75 MHz (n=3) when $p_s$ = 25 kPa.

Table 5.2: Normalized peak acoustic pressure amplitudes and their respective axial ranges for derated and tissue fields in the near-field at $p_s$=25 kPa

| | fundamental (n=1) | | second harmonic (n=2) | | third harmonic (n=3) | |
|---|---|---|---|---|---|---|
| | amplitude | position(cm) | amplitude | position(cm) | amplitude | position(cm) |
| derated fields | 1.38 | 4.26 | 0.0071 | 4.69 | 0.000064 | 5.02 |
| tissue fields | 1.39 | 4.26 | 0.0071 | 4.74 | 0.000066 | 5.03 |
| comparison | 0.99 | 0.0 | 0.99 | 0.05 | 0.97 | 0.01 |

Table 5.3: Normalized peak acoustic pressure amplitudes and their respective axial ranges for derated and tissue fields in the transition region at $p_s$=25 kPa

| | fundamental (n=1) | | second harmonic (n=2) | | third harmonic (n=3) | |
|---|---|---|---|---|---|---|
| | amplitude | position(cm) | amplitude | position(cm) | amplitude | position(cm) |
| derated fields | 0.830 | 10.1 | 0.0082 | 13.2 | 0.00013 | 14.5 |
| tissue fields | 0.837 | 10.2 | 0.0085 | 13.3 | 0.00014 | 14.6 |
| comparison | 0.99 | 0.1 | 0.96 | 0.1 | 0.93 | 0.1 |

### 5.1.2 Moderate amplitude case, $p_S$ = 250 kPa

In this section, the acoustic pressure fields generated from a source with a peak acoustic pressure amplitude of 250 kPa are examined. The water field simulations shown in Figure 5.7 illustrate the presence of harmonics along the beam axis. The axial behavior of acoustic pressure field at the fundamental frequency exhibits significant oscillation in the near-field at which the spatial peak acoustic pressure occurs 4.3 cm from the source with a normalized amplitude of 1.92. The peak acoustic pressure amplitudes of the second and third harmonics in this region are 0.146 and 0.0187, respectively, both occurring at an axial range of 4.8 cm. As a result, the harmonic content of the 4.50 and 6.75 MHz components represent 8 and 0.1% of the peak acoustic pressure amplitude at the fundamental frequency at 2.25 MHz. Steady growth of harmonics occurs in the transition region where the peak acoustic pressure amplitudes for the fundamental and the second and third harmonics are 1.89, 0.687, and 0.412 at axial ranges of 11.8, 17.3, and 19.4 cm, respectively. The harmonic content is significantly higher compared to the near-field with 36% for the second harmonic and 22% for the third harmonic of the peak acoustic pressure at the fundamental frequency.

The acoustic pressure fields for the derated fields are shown in Figure 5.8 with an expanded view of the harmonics in Figure 5.9. The derating process has reduced the peak acoustic pressures for the frequency components which now have normalized amplitudes in the near-field of 1.38, 0.0699, and 0.00621 for n=1,2 and 3, respectively, with corresponding axial ranges of 4.3, 4.7, and 5.0. Applying Equation 5.4, the resulting harmonic content for the second and third harmonics is 5 and 0.5%, respectively. Greater losses due to spatial attenuation at the last axial maxima are observed yielding peak acoustic pressures for the 2.25, 4.50, and 6.75 MHz frequencies located at 10.1, 12.6, and 13.7 cm from the transducer, respectively, with normalized amplitudes of 0.815, 0.0742, and 0.0104. The harmonic content in the transition region is reduced to 9 and 1% for the second and third harmonics, respectively.

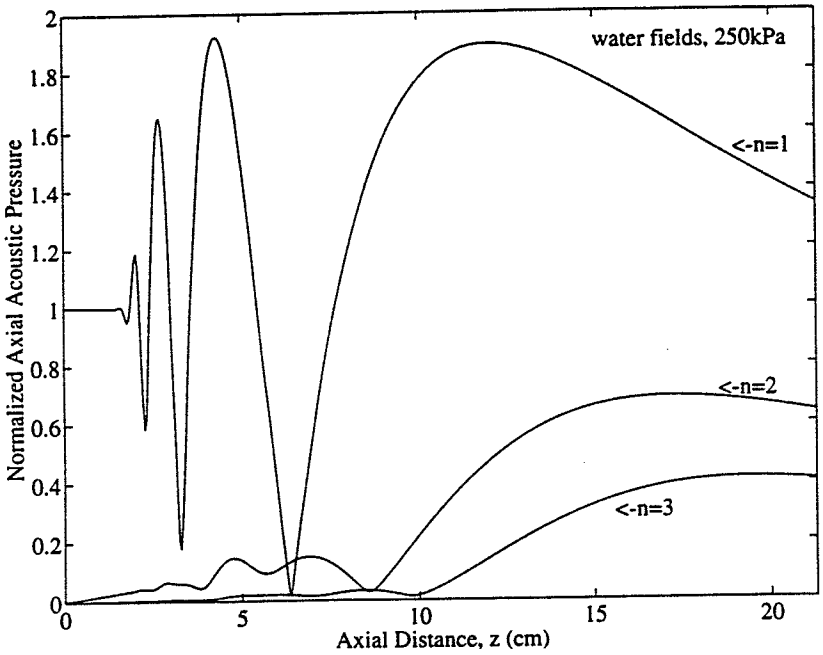


Figure 5.7: Normalized axial acoustic pressure amplitude vs. axial distance for water fields at frequencies 2.25 (n=1), 4.50 (n=2), and 6.75 MHz (n=3) when $p_s$ = 250 kPa.

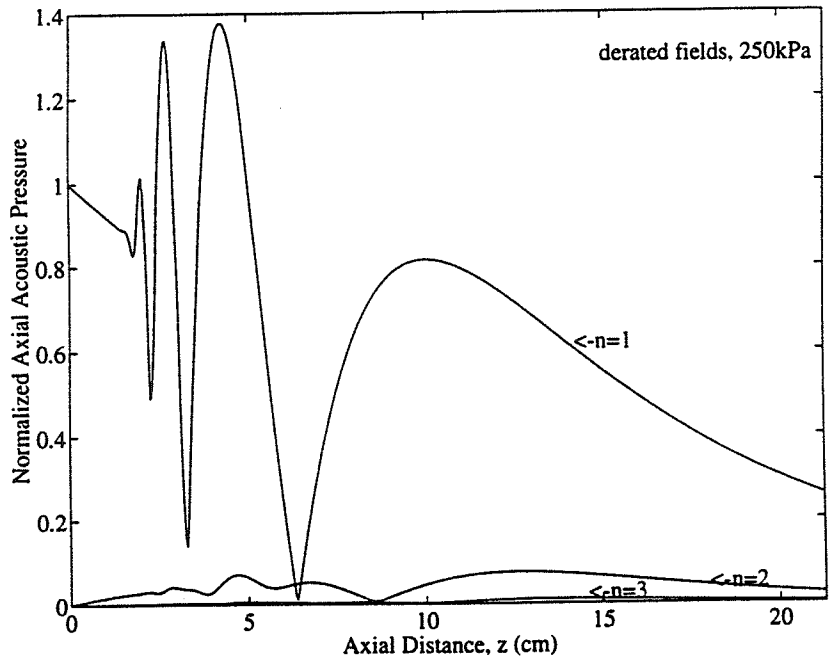


Figure 5.8: Normalized axial acoustic pressure amplitude vs. axial distance for derated fields at frequencies 2.25 (n=1), 4.50 (n=2), and 6.75 MHz (n=3) when $p_s$ = 250 kPa.

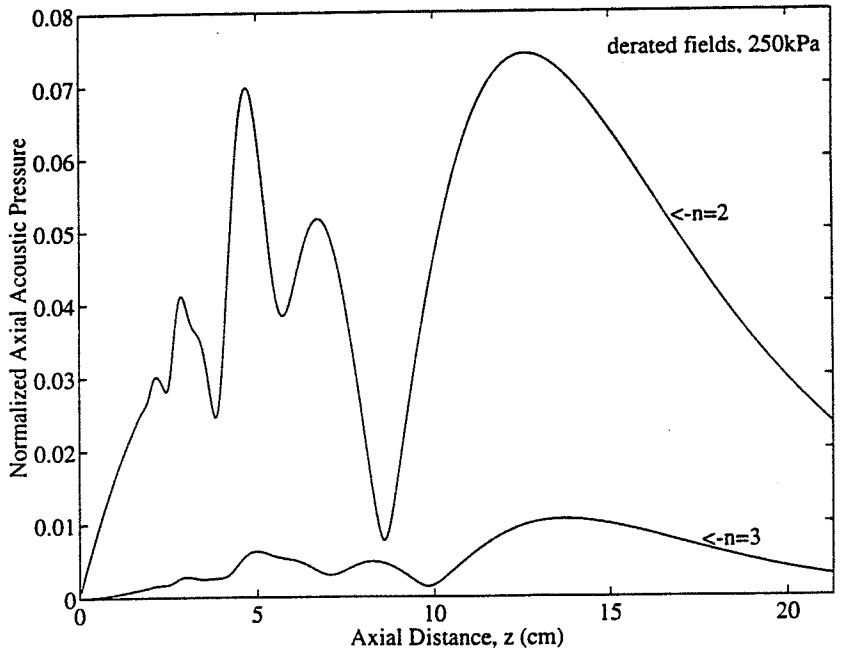


Figure 5.9: Normalized axial acoustic pressure amplitude vs. axial distance for derated fields at frequencies 4.50 (n=2) and 6.75 MHz (n=3) when $p_s$ = 250 kPa.

Figures 5.10 and 5.11 show the acoustic pressure amplitudes along the beam axis for the tissue fields. The normalized peak acoustic pressure amplitude for the fundamental is 1.39 at an axial range of 4.26 while the amplitudes for the second and third harmonics are 0.0710 and 0.00642, respectively, at ranges of 4.64 and 5.03 cm (see Table 5.4). This leads to almost the same harmonic content as the derated field case with the second and third harmonics comprising 5 and 0.5% of the fundamental, respectively. Once again, the transition region exhibits greater harmonic presence compared to the near-field with the harmonic content for the second and third harmonics now 10 and 2% of the peak acoustic pressure amplitude at the fundamental frequency, respectively.

The acoustic pressure amplitudes along the beam axis are dominated by the fundamental frequency component for both derated and tissue fields with a source acoustic pressure of 250 kPa. In addition, the ratios of the peak acoustic pressure amplitudes are very close to unity where $p_{1,ratio}$ is 0.99 and 0.98 in the near-field and transition regions, respectively, and the

corresponding $z_{1,shift}$ is 0.0 and 0.1. The ratios of the acoustic pressures for the second and third harmonics in the near-field are also close to unity where $p_{2,ratio}$ and $p_{3,ratio}$ are 0.98 and 0.97, respectively, while the corresponding $z_{2,shift}$ and $z_{3,shift}$ are both 0.05 cm. However, the derated fields begin to underestimate the acoustic pressure amplitudes of the tissue fields in the transition region since the ratios, $p_{2,ratio}$ and $p_{3,ratio}$, at the last axial maximum are 0.89 and 0.78, respectively. In addition, axial shifts of 0.6 and 0.8 are observed for $z_{2,shift}$ and $z_{3,shift}$, respectively, with the maximum of the derated fields located closer to the source. The combination of low peak acoustic pressure amplitudes with axial shifts moving the peaks closer to the source indicate a faster rate of attenuation. As a result, the derated fields emitted from a source with an acoustic pressure of 250 kPa leads to the underestimation of tissue fields with the greatest deviations in the transition region.

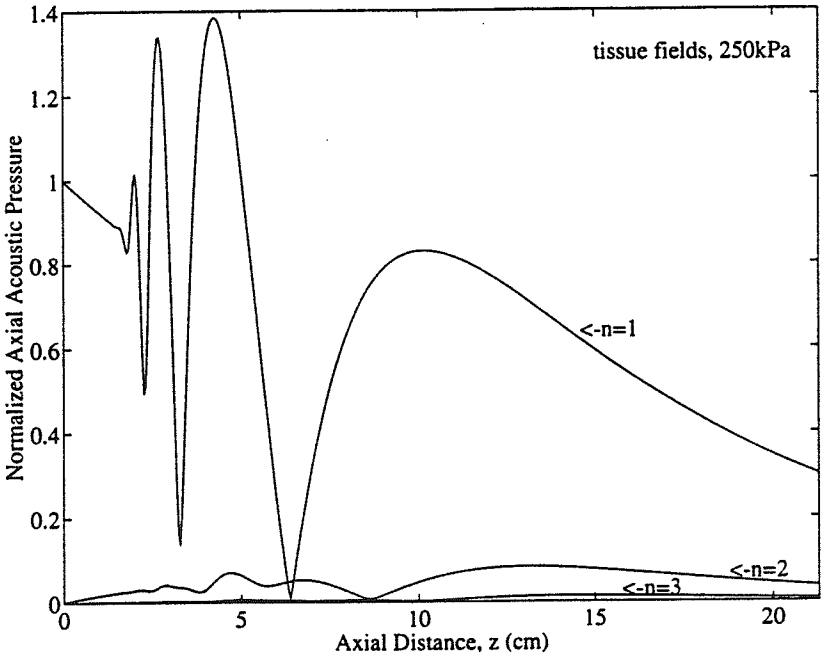


Figure 5.10: Normalized axial acoustic pressure amplitude vs. axial distance for tissue fields at frequencies 2.25 (n=1), 4.50 (n=2), and 6.75 MHz (n=3) when $p_s$ = 250 kPa.

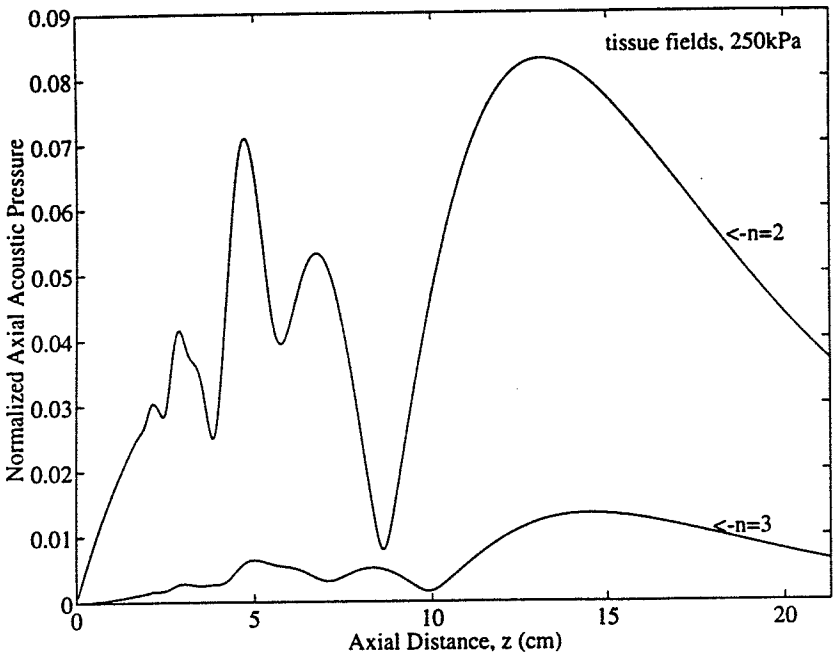


Figure 5.11: Normalized axial acoustic pressure amplitude vs. axial distance for tissue fields at frequencies 4.50 (n=2) and 6.75 MHz (n=3) when $p_s$ = 250 kPa.

Table 5.4: Normalized peak acoustic pressure amplitudes for *derated* and *tissue* fields in the near-field at $p_s$=250 kPa

| | fundamental (n=1) | | second harmonic (n=2) | | third harmonic (n=3) | |
|---|---|---|---|---|---|---|
| | amplitude | position(cm) | amplitude | position(cm) | amplitude | position(cm) |
| derated fields | 1.38 | 4.26 | 0.0699 | 4.69 | 0.00621 | 4.98 |
| tissue fields | 1.39 | 4.26 | 0.0710 | 4.74 | 0.00642 | 5.03 |
| comparison | 0.99 | 0.0 | 0.98 | 0.05 | 0.97 | 0.05 |

Table 5.5: Normalized peak acoustic pressure amplitudes for *derated* and *tissue* fields in the transition region at $p_s$=250 kPa

| | fundamental (n=1) | | second harmonic (n=2) | | third harmonic (n=3) | |
|---|---|---|---|---|---|---|
| | amplitude | position(cm) | amplitude | position(cm) | amplitude | position(cm) |
| derated fields | 0.815 | 10.1 | 0.0742 | 12.6 | 0.0104 | 13.7 |
| tissue fields | 0.831 | 10.2 | 0.0829 | 13.2 | 0.0133 | 14.5 |
| comparison | 0.98 | 0.1 | 0.89 | 0.6 | 0.78 | 0.8 |

### 5.1.2 High Amplitude Case, $p_S$ = 2.5 MPa

Thus far, only the source acoustic pressures of 25 and 250 kPa have been examined. However, when the acoustic pressure from the source is increased to 2.50 MPa, a severely distorted wave is generated in water where there is a dramatic increase in the acoustic pressure of the harmonics. The spatial peak acoustic pressures for the 2.25, 4.50, and 6.75 MHz frequency components lie in the near-field as shown in Figure 5.12 with corresponding normalized amplitudes of 1.56, 0.660, and 0.378 occurring at 4.16, 4.50, and 4.59 cm from the source. The second and third harmonics experience significant harmonic content of 42 and 24% relative to the fundamental. The peak acoustic pressure in the transition region are located

at axial ranges of 8.95, 9.28, and 9.33 cm and corresponding normalized amplitudes of 0.754, 0.406, and 0.233 for the fundamental and the second and third harmonics, respectively. Although, the peak acoustic pressure amplitudes in the transition region are smaller than the peak acoustic pressures in the near-field, the harmonic content at the last axial maximum is 53% for the second harmonic and 31% for the third harmonic of the peak acoustic pressure amplitude at the fundamental component.

The 0.3 dB/cm-MHz derating applied to the water fields results in the derated fields shown in Figure 5.13. The acoustic pressure amplitudes are provided in the first row of Tables 5.7 and 5.8 for the near-field and transition regions, respectively. The acoustic pressures in the near-field for the fundamental and the second and third harmonics are 1.22, 0.329, and 0.130, respectively, occurring at the corresponding axial ranges of 2.7, 4.5, and 4.6 cm. The harmonic content using Equation (5.4) is, therefore, 27 and 11% for n=2 and n=3, respectively. As the acoustic pressures of the frequency components in the transition region are examined, the peak amplitudes at 2.25, 4.50, and 6.75 MHz are 0.386, 0.099, and 0.012, respectively, located 8.4, 9.0, and 9.1 cm from the source. The corresponding harmonic content for n=2 and n=3 is 26 and 3%, respectively, which are now lower compared to the near-field of the peak acoustic pressure amplitude at the fundamental component.

The normalized acoustic pressure amplitudes for the tissue fields are shown in Figure 5.14. The oscillations of the peak acoustic pressure in the near-field are also the spatial peaks at located 2.7, 4.6, and 4.7 cm for the source for the frequency components at 2.25, 4.50, and 6.75 MHz, respectively, with normalized amplitudes of 1.25, 0.426, and 0.226. The resulting harmonic content is 34 and 18% for n=2 and n=3, respectively. In the transition region, however, the harmonic components have normalized peak acoustic pressures of 0.194 and 0.113 at axial ranges of 10.3 and 11.0 cm for frequencies at 4.50 and 6.75 MHz, respectively, while the fundamental has an amplitudes of 0.500 at a range of 8.80 cm. This results in a harmonic content of 39% for n=2 and 23% and n=3.

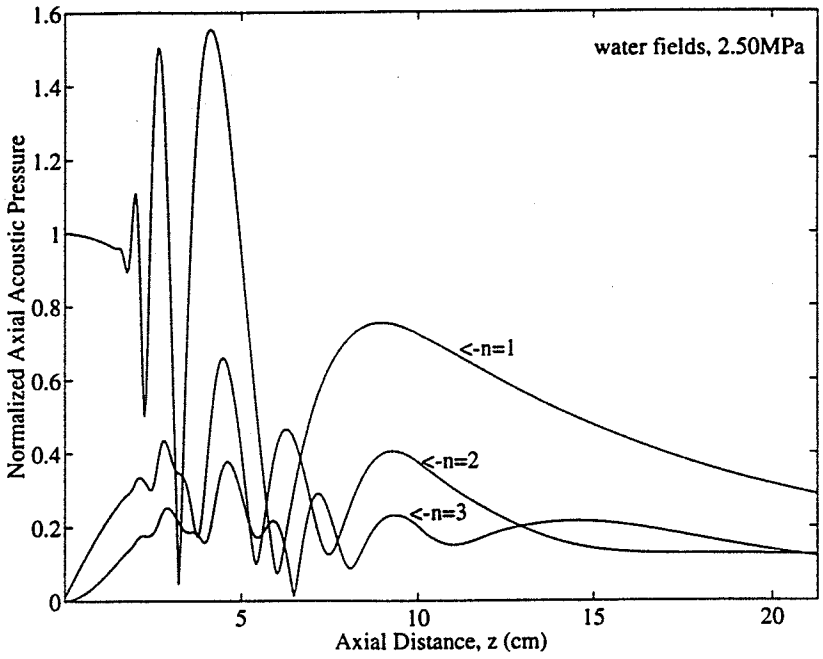


Figure 5.12: Normalized axial acoustic pressure amplitude vs. axial distance for water fields at frequencies 2.25 (n=1), 4.50 (n=2), and 6.75 MHz (n=3) when $p_s$ = 2.50 MPa.

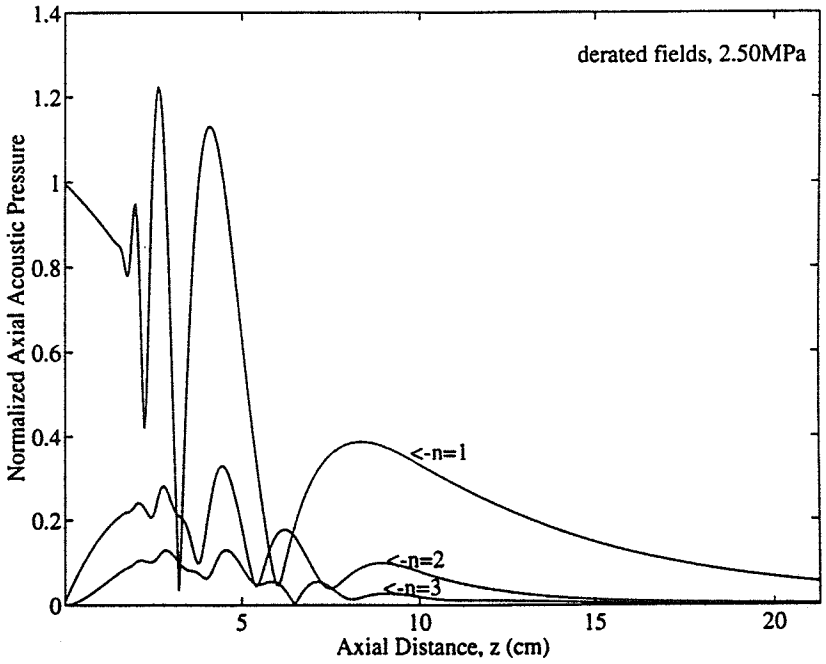


Figure 5.13: Normalized axial acoustic pressure amplitude vs. axial distance for derated fields at frequencies 2.25 (n=1), 4.50 (n=2), and 6.75 MHz (n=3) when $p_s$ = 2.50 MPa.

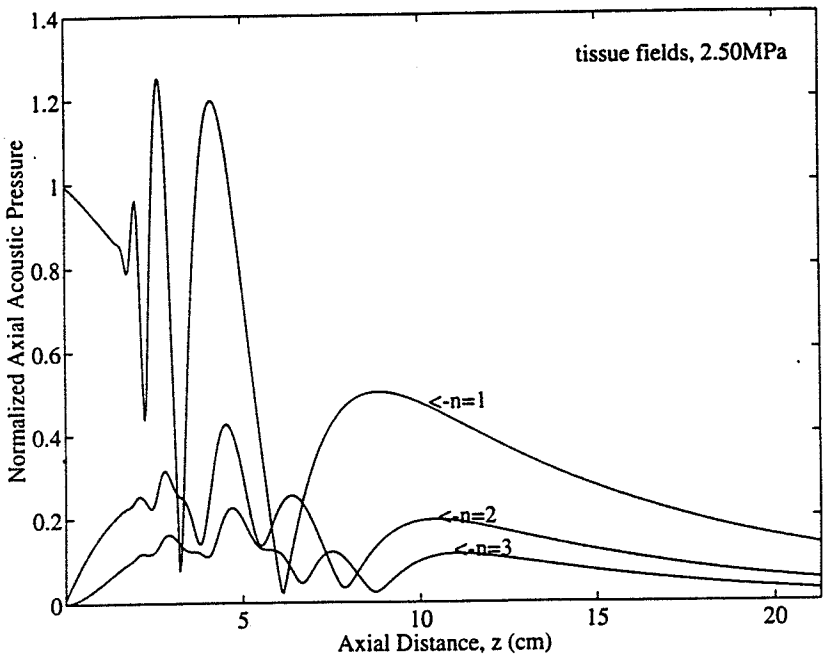


Figure 5.14: Normalized axial acoustic pressure amplitude vs. axial distance for tissue fields at frequencies 2.25 (n=1), 4.50 (n=2), and 6.75 MHz (n=3) when $p_s$ = 2.50 MPa.

As just shown, the harmonic content of acoustic pressure amplitudes are significant throughout the axial beam at an acoustic source pressure of 2.50 MPa. However, the derated and tissue fields are now analyzed to compare agreement between the two fields at the high source level (Tables 5.6 and 5.7). The peak acoustic pressure for the derated fields in the near-field at the fundamental is the only value that compares favorable with the acoustic pressure for the corresponding tissue fields, i.e., $p_{1,ratio}$=0.98 and $z_{1,shift}$=0.0. However, the peak acoustic pressures between the derated and tissue fields of the harmonics begin to deviate significantly in this region since the ratios for $p_{2,ratio}$ and $p_{3,ratio}$ are now 0.77 and 0.58 respectively with corresponding axial shifts of 0.10 and 0.14 cm. The derated and tissue fields are further degraded in the transition region where the last axial maxima have $p_{1,ratio}$= 0.77, $p_{2,ratio}$=0.51, and $p_{3,ratio}$=0.11. In addition, the axial shifts are also quite severe with differences of 0.4, 1.4 and 1.9 for $z_{1,shift}$, $z_{2,shift}$, and $z_{3,shift}$, respectively.

Table 5.6: Normalized peak acoustic pressure amplitudes for derated and tissue fields in the near-field at $p_s$=2.50 MPa

| | fundamental (n=1) | | second harmonic (n=2) | | third harmonic (n=3) | |
|---|---|---|---|---|---|---|
| | amplitude | position(cm) | amplitude | position(cm) | amplitude | position(cm) |
| derated fields | 1.22 | 2.66 | 0.329 | 4.45 | 0.130 | 4.55 |
| tissue fields | 1.25 | 2.66 | 0.426 | 4.55 | 0.226 | 4.69 |
| comparison | 0.98 | 0.0 | 0.77 | 0.10 | 0.58 | 0.14 |

Table 5.7: Normalized peak acoustic pressure amplitudes for derated and tissue fields in the transition region at $p_s$=2.50 MPa

| | fundamental (n=1) | | second harmonic (n=2) | | third harmonic (n=3) | |
|---|---|---|---|---|---|---|
| | amplitude | position(cm) | amplitude | position(cm) | amplitude | position(cm) |
| derated fields | 0.386 | 8.37 | 0.099 | 8.95 | 0.012 | 9.1 |
| tissue fields | 0.500 | 8.80 | 0.19 | 10.3 | 0.113 | 11.0 |
| comparison | 0.77 | 0.43 | 0.51 | 1.4 | 0.11 | 1.9 |

Tables 5.6 and 5.7 summarize the simulation of the acoustic pressure amplitudes in derated and tissue fields and compares the peak amplitudes at a source pressure of 2.50 MPa. It is evident that the linear derating scheme results in faster attenuation resulting an underestimation of the peak acoustic pressure amplitudes of tissue fields using tissue parameters.

## 5.2 Discussion

According to linear theory, as the acoustic pressure at the source is increased the acoustic pressure fields will increase proportionately. However, when dealing with high amplitude waves in a low-loss, nonlinear medium such as water, the acoustic waves will begin to saturate. As a result, there will no longer be a one-to-one correspondence between the propagated wave and the source. Rather, more energy will be transferred to the harmonic components resulting in greater waveform distortion. However, for an attenuating medium, significantly higher acoustic source pressures are necessary before the onset of acoustic saturation. In addition, the growth of harmonics is inhibited. Since attenuation losses are frequency dependent, this results in less overall attenuation than occurring in a lossless medium where more energy is transferred to higher frequencies. As a result, for an attenuating medium the fundamental component predominates. However, the FDA derating scheme [20] assumes a linear wave propagation model which was shown to be inadequate when finite amplitude waves are considered. Linear models have been shown to underestimate the *in situ* acoustic pressure levels as suggested by the AIUM bioeffects committee [1]. As a result, extreme caution must be exercised when water calibrations are performed to estimate the fields in tissue.

# CHAPTER 6
# CONCLUSIONS

The calibration scheme established by the FDA based on linear wave propagation that is used to predict *in situ* exposure was examined. The main goal was to assess the derating scheme which is based on acoustic pressure measurements made in water. To account for wave distortion, the well-established Khokhlov-Zabolotskaya-Kuznetsov model for nonlinear, diffractive wave propagation in thermoviscous media was applied to predict the harmonic content along the beam axis of a plane piston transducer.

The behavior of the wave was shown to be dependent on pressure at the source since this quantity is inversely proportional to the discontinuity distance, $\ell_d$. That is, as the transmitted pressure amplitude is increased, the shock distance is decreased resulting in greater waveform distortion. However, attenuation due primarily to thermoviscous losses reduced the effects of nonlinearity since the higher-frequency components of the acosutic pressure were attenuated at a faster rate.

Waveform distortion was shown not to be appreciable in water at lower source amplitudes. As a result, the *in situ* acoustic pressure fields using the FDA derating scheme did not exhibit significant deviation for the first three harmonics from the nonlinear fields generated using tissue field parameters. However, the presence of harmonics was noticeable in water at amplitude levels typically employed in diagnostic ultrasound. As the linear derated fields were compared to tissue field propagation, there was disagreement between the acoustic pressure amplitudes of the first three harmonics in the near-field with the greatest differences occurring in the transition region. As the amplitude was increased, the acoustic pressure fields generated in water began to saturate. As a result, the linearly derated fields no longer accurately described fields in lossy media which resulted in the underestimation of the pressure fields in tissue.

The current trends of ultrasound equipment have been to increase the output levels delivered since no biological effects have been produced in the clinical setting. This does not mean, however, that damage is not possible. As a result, accurate models for the emitted fields are needed to assess the safe operating levels.

Further work in this field is needed to account for a more realistic clinical setting. For instance, the theory must be modified to include focused sound beams that are used in virtually all examinations. In addition, the homogeneous model does not reflect the typical propagation path for an acoustic wave. Rather, a wave must pass through skin, fat, muscle, and even amniotic fluid before it reaches the region of interest. As a result, these layers should be included in future nonlinear modeling. Once an accurate field description has been achieved, the intensity distribution can be subsequently calculated and used to estimate temperature rise.

In summary, FDA derating criteria do not reflect the fields present in situ when a nonlinear propagation model is considered. Only through accurate prediction of finite amplitudes waves in tissue can the safety of diagnostic ultrasound be guaranteed.

# REFERENCES


[1] American Institute of Ultrasound in Medicine, *Bioeffects and Safety of Diagnostic Ultrasound*. Rockville MD: AIUM Publications, 1993.

[2] S. I. Aanonsen, T. Barkve, J. N. Tjotta, and S. Tjotta, "Distortion and harmonic generation in the nearfield of a finite amplitude sound beam," *J. Acoust. Soc. Am.*, vol. 75, pp.749-78, 1984.

[3] S. I. Aanonsen, "Numerical computation of the nearfield of a finite amplitude sound beam," Rep. No. 73, Department of Mathematics, University of Bergen, Norway, 1983.

[4] A. C. Baker, K. Anastasiadis, and V. F. Humphrey, "The nonlinear pressure field of a plane circular piston: Theory and experiment," *J. Acoust. Soc. Am.*, vol. 84, pp. 1483-1487, 1988.

[5] E. L. Carstensen, W. K. Law, N. D. McKay, and T. G. Muir, "Demonstration of nonlinear acoustical effects at biomedical frequencies and intensities," *Ultrasound in Medicine and Biology* , vol. 6, pp. 359-68, 1980.

[6] D. T. Blackstock, "Thermovicous attenuation of plane, periodic, finite amplitude sound waves," *J. Acoust. Soc. Am.*, vol. 36, pp. 534-42, 1964.

[7] D. T. Blackstock, "Connection between the Fay and Fubini solutions for plane sound waves of finite amplitude," *J. Acoust. Soc. Am.*, vol. 39, pp. 1019-26, 1966.

[8] D. T. Blackstock, "Nonlinear acoustics with applications to underwater sound," Lecture notes for summer graduate course in ocean acoustics, Catholic University of America, Washington D.C., 1974.

[9] M. E. Haran and B. D. Cook, "Distortion of finite amplitude ultrasound in lossy media," *J. Acoust. Soc. Am.*, vol. 73, pp. 774-79, 1983.

[10] L. E. Kinsler, A. R. Frey, A. B. Coppens, and J. V. Sanders, *Fundamentals of Acoustics,* 3rd edition. New York: John Wiley and Sons, 1982.

[11] B. K. Novikov, O. V. Rudenko, and V. I. Timoshenko, *Nonlinear Underwater Acoustics.* New York: American Institute of Physics, 1987.

[12] O. V. Rudenko and S. I. Soluyen, *Theoretical Foundations of Nonlinear Acoustics.* New York: Consultants Bureau, 1977.

[13] P. M. Morse and K. U. Ingard, *Theoretical Acoustics.* New York: McGraw Hill, 1968.

[14] P. T. Christopher and K. J. Parker, "New approaches in nonlinear diffractive wave propagation,"*J. Acoust. Soc. Am.*, vol. 90, pp. 200-219, 1991.

[15] G. D. Smith, *Numerical Solutions of Partial Differntial Equations: Finite Difference Methods.* Oxford: Oxford University Press, 1978.

[16] V. A. Shutilov, *Fundamental Physics of Ultrasound.* New York: Gordon and Breach Science Publishers, 1988.

[17] D. J. Watmough and W. M. Ross , "Clinical and scientific aspects," in *Hyperthermia*, D. J. Watmough and W. M. Ross, Eds. London: Blackie, 1986, pp. 1-12.

[18] R. C. Preston, A. Shaw, and B. Zeqiri, "Prediction of *in situ* exposure to ultrasound: An acoustical attenuation method," *Ultrasound Med. & Biol.*, vol. 17, no. 4, pp. 317-32, 1991.

[19] D. S. Ellis, "The general solution for estimating ultrasonically induced tisue heating," M.S. thesis, University of Illinois at Urbana-Champaign, Urbana, 1992.

[20] American Institute of Ultrasound in Medicine, *Acoustic Output Measurement and Labeling Standard for Diagnostic Ultrasound Equipment.* Rockville MD: AIUM Publications, 1992.

[21] American Institute of Ultrasound in Medicine, *Standard Real-Time Dispaly of Thermal and Mechanical Acoustic Output Indices on Diagnostic Ultrasound Equipment.* Rockville MD: AIUM Publications, 1992.

[22] H. Kuttruff, *Ultrasonics: Fundamentals and Applications.* New York: Elsevier Applied Science, 1991.

[23] M. J. Haney and W. D. O'Brien, Jr., "Temperature dependency of ultrasonic propagation properties in biological materials," in *Tissue Characterization with Ultrasound: Volume I*, J. F. Greenleaf, Editor. Boca Raton: CRC Press, 1986, pp. 15-56.

# APPENDIX A

# KZK SIMULATION PROGRAMS

```
/* kzk1.c */

#include <stdio.h>
#include <stdlib.h>
#include <math.h>
#include <malloc.h>
#include "mystruct.h"

#define PI 3.141592654


/*************************************************************************
 *    MAIN                                                               *
 *************************************************************************/
void main()
{
      double a, f, co, po;
      double pressure;
      double BoA, ld;
      double alpha, ro;
      double fnum;                  /* frequency dependence */
      double wavenum;

      double abp;             /* params */
      double nonl;
      double gain;
      double delta;
      double r;
      double s;               /* compression factor */
      int m;                        /* number of harmonics */
                              /* used in calculations*/

      double zstep;                 /* steps */
      double xstep;
      int imax;

      double zmax;
      double xmax;
      int filout;             /* # of harmonics printed */

      long int j;
      int i, eta;
      double z;               /* axial coordinate */
      int k, l, n;
      double ampl, phl;

      char  summary[20];
      FILE  *fsumm;

      char  n1[20], n2[20], n3[20];
```

```
      FILE  *fn1, *fn2, *fn3;

      char  dfile3[20];
      FILE  *fptr3;
      char  dfile2[20];
      FILE  *fptr2;
      char  dfile4[20];
      FILE  *fptr4;
      char  strnum[5];

extern void initial();
extern void profile();
extern void init_matrix();
extern void next();
extern double phase();
extern double ampltud();
extern void ltoa();

MxStruct *matrix;
CfStruct *coef;

matrix = (MxStruct *)calloc(1, sizeof(MxStruct));
coef = (CfStruct *)calloc(1, sizeof(CfStruct));


/***********************************
 *    INITIALIZE VARIABLES          *
 ***********************************/

      scanf("%le %*[^\n]\n", &pressure);
      scanf("%le %*[^\n]\n", &a);
      scanf("%le %*[^\n]\n", &f);
      scanf("\n");
      scanf("%le %*[^\n]\n", &BoA);
      scanf("%le %*[^\n]\n", &alpha);
      scanf("%le %*[^\n]\n", &fnum);
      scanf("%le %*[^\n]\n", &co);
      scanf("%le %*[^\n]\n", &po);
      scanf("\n");
      scanf("%le %*[^\n]\n", &zmax);
      scanf("%le %*[^\n]\n", &zstep);
      scanf("%le %*[^\n]\n", &xmax);
      scanf("%le %*[^\n]\n", &xstep);
      scanf("%d %*[^\n]\n", &m);


      wavenum = 2*PI*f/co;           /* wave number    */
      ro = (wavenum*a*a)/2;                /* Rayleigh distance    */

                              /* discontinuity distance */
      ld = 2*po*co*co/( (2 + BoA)*(2*PI*f)*pressure );

      gain = 1/(alpha * ld);         /* Goldberg's number     */
      nonl = 2*ro/ld;                /* A in sims             */

      s = 1.;
      delta = 1.;
      r = zstep/(xstep*xstep);
```

```
        imax = (int) (xmax/xstep);
        j=1;
        k=1;
        filout = 3;


strcpy(summary, "README.txt");
if (( fsumm=fopen(summary, "a")) == NULL)
      { printf("COULD NOT OPEN README.txt");
        exit(0); }
fprintf(fsumm,"INITIAL CONDITIONS:\n\n");
fprintf(fsumm,"\tINITIAL PRESSURE\t p = %.3le\n", pressure);
fprintf(fsumm,"\tTDR radius\t\t a = %.3le\n", a);
fprintf(fsumm,"\tWave number\t\t k = %.3le\n", wavenum);
fprintf(fsumm,"\tLinear Absorption\t alpha = %.3le\n", alpha);
fprintf(fsumm,"\tFrequency dependence\t b = %.3le\n", fnum);
fprintf(fsumm,"\tDiscont. dist\t\t ld = %.3le\n", ld);
fprintf(fsumm,"\tRayleigh length\t\t ro = %.3le\n", ro);
fprintf(fsumm,"\tspeed of sound\t\t co = %.3le\n", co);
fprintf(fsumm,"\tdensity of medium\t po = %.3le\n", po);
fprintf(fsumm,"\tNONLINEARITY PARAM\t B/A = %.3le\n\n", BoA);

fprintf(fsumm,"\tGAMMA = %.3le\n", gain);
fprintf(fsumm,"\tA = %.3le\n\n", nonl);
fprintf(fsumm,"\tZmax = %.3le\n\t Zstep = %.3le\n", zmax, zstep);
fprintf(fsumm,"\tXmax = %.3le\n\t Xstep = %.3le\n", xmax, xstep);
fprintf(fsumm,"\tImax = %d\n\t M = %d\n", imax, m);
fprintf(fsumm,"\tR = %.3le\n", r);
fclose(fsumm);

      strcpy(n1, "AMP1.dat");
      strcpy(n2, "AMP2.dat");
      strcpy(n3, "AMP3.dat");

      init_matrix(matrix, imax);
      initial(coef, imax, xstep, abp, nonl, gain, delta, r, s, m);


      while ( j*zstep <= zmax )
      {
            next(coef, matrix, abp, nonl, gain, delta, r, s, m, zstep,
                                          imax, j, fnum);
            if ( fabs(coef->g[1][0]) > 10. )
            {
                  printf("INSTABILTIY OCCURRED!\n");
                  strcpy(dfile3, "INSTAB.dat");
                  ltoa(j, strnum);
                  strcat(dfile3, strnum);
                  strcat(dfile3, ".dat");
                  if (( fptr3=fopen(dfile3, "w")) == NULL)
                  { printf("COULD NOT OPEN *.dat");
                    exit(0); }
                  for (n = 1; n<= filout; n++)
                  {     fprintf(fptr3, "J=%ld\tN=%d\n", j, n);
                        for (i = 0; i < imax; i++)
                              fprintf(fptr3, "G(%d,%d)=%.3le\t
                                    H(%d,%d)=%.3le\n", n, i,
                                     coef->g[n][i], n, i, coef->h[n][i]);
```

```
                }
                fclose(fptr3);
        }

        if ( (fmod( (float)j, 5.) == NULL) )
        {
                profile(coef, s, m, j);

/* WRITE DATA TO FILES */
/* 1st harmonic        */
                n=1;
                if (( fn1=fopen(n1, "a")) == NULL)
                { printf("COULD NOT OPEN AMP.dat");
                  exit(0); }

                fprintf(fn1, "\n%ld ", j);

                for ( eta = 0; eta < imax; eta++)
                {
                      ampl=ampltud(coef->g[n][eta],
                            coef->h[n][eta], s);
                      fprintf(fn1, "%.3le ", ampl);
                }
                  for ( eta = 0; eta < imax; eta++)
                  {
                          ph1=phase(coef->g[n][eta],
                            coef->h[n][eta],s,n,eta,xstep);
                          fprintf(fn1, "%.3le " , ph1);
                  }
                  fclose(fn1);

/* 2nd harmonic        */      n=2;
                  if (( fn2=fopen(n2, "a")) == NULL)
                  { printf("COULD NOT OPEN AMP.dat");
                    exit(0); }

                fprintf(fn2, "\n%ld ", j);

                for ( eta = 0; eta < imax; eta++)
                {
                      ampl=ampltud(coef->g[n][eta],
                            coef->h[n][eta], s);
                      fprintf(fn2, "%.3le ", ampl);
                }
                  for ( eta = 0; eta < imax; eta++)
                  {
                          ph1=phase(coef->g[n][eta],
                            coef->h[n][eta],s,n,eta,xstep);
                          fprintf(fn2, "%.3le " , ph1);
                  }
                  fclose(fn2);

/* 3rd harmonic      */
                  n=3;
                  if (( fn3=fopen(n3, "a")) == NULL)
                  { printf("COULD NOT OPEN AMP.dat");
                    exit(0); }
```

```
                                fprintf(fn3, "\n%ld ", j);

                                for ( eta = 0; eta < imax; eta++)
                                {
                                        ampl=ampltud(coef->g[n][eta],
                                                coef->h[n][eta], s);
                                        fprintf(fn3, "%.3le ", ampl);
                                }
                                for ( eta = 0; eta < imax; eta++)
                                {
                                        phl=phase(coef->g[n][eta],
                                          coef->h[n][eta],s,n,eta,xstep);
                                        fprintf(fn3, "%.3le " , phl);
                                }

                                fclose(fn3);

/* END WRITE DATA TO FILES */

                        k++;
                }


                j++;            /* next axial step */
        }
}

#include <stdio.h>
#include <stdlib.h>
#include <math.h>
#include <malloc.h>
#include "mystruct.h"

void next();

/*************************************************************
 *              NEXT                                         *
 *************************************************************/
void next(coef, matrix, abp, nonl, gain, delta, r, s, m, zstep, imax, j,
fnum)

CfStruct *coef;
MxStruct *matrix;
double abp, nonl, gain, delta, r, s, zstep;
double fnum;
int imax;
int m;
long int j;

{
double *gfn, *hfn, *gnew, *hnew;
double norm, mag;
int l, lmax=20;
int i, n;
double c2;
double eps, fact;

char dfile6[20];
```

```
FILE *fptr6;
char dfile7[20];
FILE *fptr7;
char dfile8[20];
FILE *fptr8;
char snum[5];

double sumg();
double sumh();
double mult();
extern void ltoa();

gfn = (double *)calloc(501, sizeof(double));
hfn = (double *)calloc(501, sizeof(double));
gnew = (double *)calloc(501, sizeof(double));
hnew = (double *)calloc(501, sizeof(double));


      if ( gfn==NULL || hfn==NULL || gnew==NULL || hnew==NULL)
      {
            printf("****** error callocing in NEXT.C **********");
            exit(0);
      }

      strcpy(dfile6, "ITER.dat");
      if ( (fptr6 = fopen(dfile6, "a")) == NULL)
      {
            printf("******** Error in FILE I/O in NEXT.C *****");
            exit(0);
      }

      for (n = 1; n <= m; n++)
      {
            c2 = (zstep*n*nonl)/4;
            for (i = 0; i < imax; i++)
            {
                  gfn[i] = coef->g[n][i] + c2*sumg(coef,n,m,i);
                  hfn[i] = coef->h[n][i] + c2*sumh(coef,n,m,i);
                  gnew[i] = coef->g[n][i];
                  hnew[i] = coef->h[n][i];
            }

            l = 1;
            fact = 1./( 1+pow((double)n,fnum)*zstep*nonl/(2*gain) );
            norm = 1.;
            eps = 1.e-5;
            while (norm >= eps && l <= 30)
            {
                  for (i = 0; i < imax; i++)
                  {
                        gnew[i] = fact*(gfn[i]+r*mult(matrix, imax, hnew,
i)/(4*n));
                  }

                  for (i = 0; i < imax; i++)
                  {
                        hnew[i] = fact*(hfn[i]-r*mult(matrix, imax, gnew,
i)/(4*n));
```

```
                }

                norm = 0.;

                for (i = 0; i < imax; i++)
                {
                        mag = fabs( gnew[i] - coef->g[n][i] );
                        if (mag > norm)
                                norm = mag;
                        coef->g[n][i] = gnew[i];
                        coef->h[n][i] = hnew[i];
                }
                l++;
        }

        if (l > lmax)
                fprintf(fptr6, "J = %ld\tHarmonic = %d\tIteration = %d\t
NORM = %le\n", j, n, l, norm);
    /*printf("NEXT.c:\t G(%d,0) = %.3le\t H(%d,0) = %.3le\n",
                n, coef->g[n][0], n, coef->h[n][0]); */
    }

    fclose(fptr6);
    free(gnew);
    free(hnew);
    free(gfn);
    free(hfn);
}

/*************************************************************
 *          SUMG                                             *
 *************************************************************/
double sumg(coef, n, m, i)
    CfStruct *coef;
    int n, m, i;
{
int inx;
double sum;

    sum = 0.;
    for (inx = 1; inx <= (n - 1); inx++)
        sum = sum + coef->g[n - inx][i]*coef->g[inx][i] -
                coef->h[n-inx][i]*coef->h[inx][i];
    sum = sum/2;
    for (inx = m; inx >= (n+1); inx--)
    {
        sum = sum - coef->g[inx-n][i]*coef->g[inx][i] -
                coef->h[inx-n][i]*coef->h[inx][i];
    }
    return(sum);
}


/*************************************************************
 *          SUMH                                             *
 *************************************************************/
double sumh(coef, n, m, i)
    CfStruct *coef;
```

```
        int n, m, i;
{
int inx;
double sum;

        sum = 0.;
        for (inx = 1; inx <= (n - 1); inx++)
        {
                sum = sum + coef->g[n - inx][i]*coef->h[inx][i] +
                            coef->h[n-inx][i]*coef->g[inx][i];
        }
        sum = sum/2;
        for (inx = m; inx >= (n+1); inx--)
        {
/*              printf("SUMH:\t N = %d\t INX = %d\n", n, inx);
*/              sum = sum + coef->h[inx-n][i]*coef->g[inx][i] -
                            coef->g[inx-n][i]*coef->h[inx][i];
        }
        return(sum);
}


/*************************************************************
 *          MULT                                             *
 *************************************************************/
double mult(mx, imax, x, i)
        MxStruct *mx;
        int imax, i;
        double *x;
{
double mt;
/*      if (i < 1 || i > imax)
        {
                printf("NO WAY:\t I = %d\n", i);
                mt = .1e20;
        }
        else */ if (i == 0)
                mt = mx->diag[i]*x[i] + mx->beta[i]*x[i+1];
        else if (i == (imax-1))
                mt = mx->alfa[i]*x[i-1] + mx->diag[i]*x[i];
        else
                mt = mx->alfa[i]*x[i-1] + mx->diag[i]*x[i] +
                                          mx->beta[i]*x[i+1];
/*printf("MULT:\t I=%d\tALFA = %.3le\t BETA = %.3le\t DIAG = %.3le\n", i,
mx->alfa[i], mx->beta[i], mx->diag[i]); */
return(mt);
}

#include <stdio.h>
#include <stdlib.h>
#include <math.h>
#include <malloc.h>
#include "mystruct.h"


void initial(coef, imax, ustep, abp, nl, gain, delta, r, s, m)
        CfStruct *coef;
        int imax, m;
```

```
      double abp, nl, gain, delta, r, s, ustep;

{

double iniamp();
double iniphase();
extern double ampltud();
extern double phase();

int i, n;
double u;
char dfile4[20];
FILE *fptr4;

      strcpy(dfile4, "INITIAL.dat");
      if (( fptr4 = fopen(dfile4, "w")) == NULL)
      {
            printf("Could not open %s", dfile4);
            exit(0);
      }

      for (i = 0; i <= imax-1; i++)
      {
            u = i*ustep;
            coef->g[1][i] = iniamp(u, delta, gain) * cos(iniphase(u,
delta));
            coef->h[1][i] = iniamp(u, delta, gain) * sin(iniphase(u,
delta));
            fprintf(fptr4, "%.3le\t %.3le\n", ampltud(coef->g[1][i], coef-
>h[1][i]), phase(coef->g[1][i], coef->h[1][i], s, n, i, ustep));

            for (n = 2; n <= m; n++)
            {
                  coef->g[n][i] = 0.;
                  coef->h[n][i] = 0.;
            }
      }
      for (i = 1; i <= m; i++)
      {
            coef->g[i][imax] = 0.;
            coef->h[i][imax] = 0.;
      }
      fclose(fptr4);

}

/*********************************************************************
 *    INIAMP()                                                       *
 *********************************************************************/
double iniamp(u, delta, gain)
      double u, delta, gain;
{
double ampl;
      if ( u < -1. || u > 1.)
            ampl = 0.;
      else
            ampl = 1.;
```

```
        return(ampl);
}

/*************************************************************************
 *    INIPHASE()                                                         *
 *************************************************************************/
double iniphase(u, delta)
        double u;
        double delta;
{
double pe;

        pe = 0.;
        return(pe);
}

#include <stdio.h>
#include <stdlib.h>
#include <math.h>
#include <malloc.h>
#include "mystruct.h"

void init_matrix(mx,imax)
        MxStruct *mx;
        int imax;
{
int i,k;
        mx->diag[0] = -4.;
        mx->alfa[0] = 0.;
        mx->beta[0] = 4.;

        for (k = 1; k <= (imax - 2); k++)
        {
                mx->diag[k] = -2.;
                mx->alfa[k] = 1. - 1/(double) (2*k);
                mx->beta[k] = 1. + 1/(double) (2*k);
        }
        mx->diag[imax-1] = -2.;
        mx->alfa[imax-1] = 1. - 1/(double)(2*(imax-1));
        mx->beta[imax-1] = 0.;
}

#include <stdio.h>
#include <stdlib.h>
#include <math.h>
#include <malloc.h>
#include "mystruct.h"

void profile(coef, s, m, j)
        CfStruct *coef;
        double s;
        int m;
        long int j;
{
double sum;
double step;
int i, n;
char dfile[30];
```

```
FILE *fptr;
char nstr[5];
extern void ltoa();

      strcpy(dfile, "PROFILE");
/*    ltoa(j, nstr);
      strcat(dfile, nstr);
*/
      strcat(dfile, ".dat");
      if ( ( fptr = fopen(dfile, "a")) == NULL) {
            printf("ERROR OPENING PROF.dat");
            exit(0);
      }
      fprintf(fptr,"%ld ", j);
      step = asin(1.)/50;
      for (i = -100; i <= 100; i++)
      {
            sum = 0;
            for (n = (m-2); n >= 1; n--)
                  sum = sum + coef->g[n][0]*sin(step*i*n)/s +
                              coef->h[n][0]*cos(step*i*n)/s;
            fprintf(fptr,"%.3le ", sum);
      }
      fprintf(fptr,"\n");
      fclose(fptr);
}
```